AD-A069 648 AIR FORCE MATERIALS LAB WRIGHT-PATTERSON AFB OH F/G 11/6
THE INTERFEROMETRIC MEASUREMENT OF NEAR CRACK TIP DISPLACEMENTS--ETC(U)
MAR 79 J W JONES

UNCLASSIFIED AFML-TR-78-159 NL

1 OF 1
AD A069 648

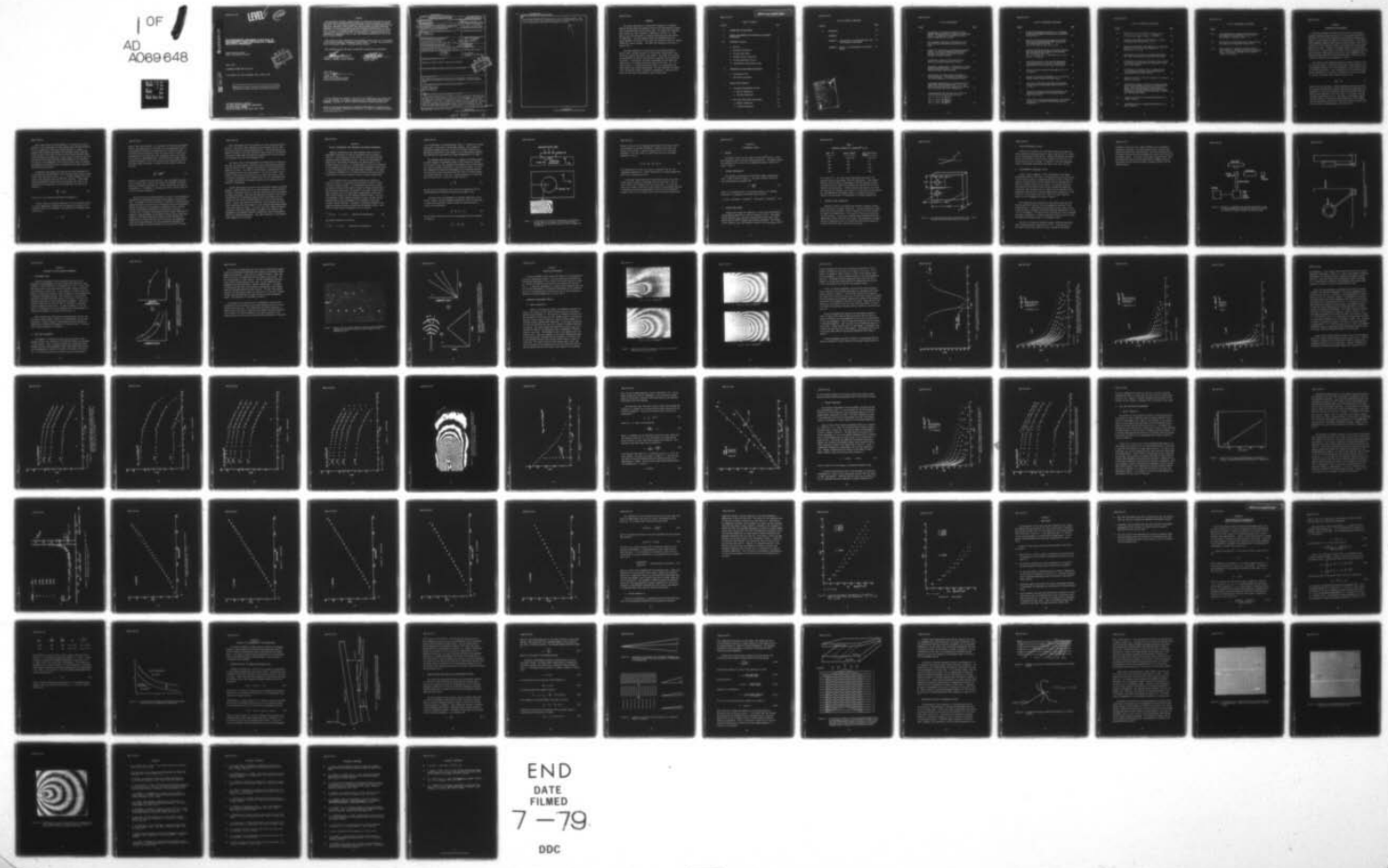

END
DATE FILMED
7-79
DDC

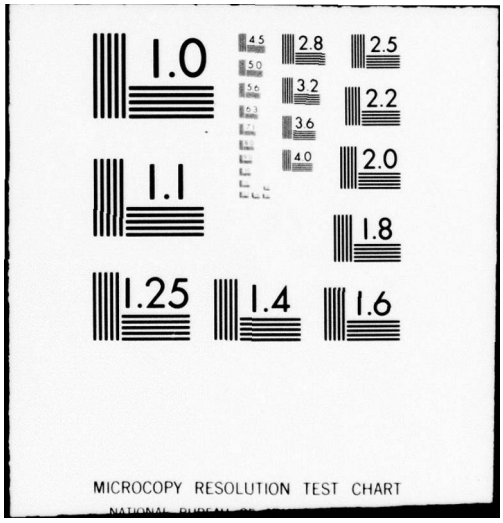
1.0
1.1
1.25
1.4
1.6
1.8
2.0
2.2
2.5
2.8
3.2
3.6
4.0
4.5
5.0
5.6
6.3
MICROCOPY RESOLUTION TEST CHART

AFML-TR-78-159

LEVEL II

THE INTERFEROMETRIC MEASUREMENT OF NEAR CRACK TIP DISPLACEMENTS IN A NICKEL BASE SUPERALLOY AT AMBIENT AND ELEVATED TEMPERATURES

Metals Behavior Branch
Metals and Ceramics Division

March 1979

TECHNICAL REPORT AFML-TR-78-159

Final Report for Period December 1976 to April 1978

Approved for public release; distribution unlimited.

AIR FORCE MATERIALS LABORATORY
AIR FORCE WRIGHT AERONAUTICAL LABORATORIES
AIR FORCE SYSTEMS COMMAND
WRIGHT-PATTERSON AIR FORCE BASE, OHIO 45433

NOTICE

When Government drawings, specifications, or other data are used for any purpose other than in connection with a definitely related Government procurement operation, the United States Government thereby incurs no responsibility nor any obligation whatsoever; and the fact that the government may have formulated, furnished, or in any way supplied the said drawings, specifications, or other data, is not to be regarded by implication or otherwise as in any manner licensing the holder or any other person or corporation, or conveying any rights or permission to manufacture, use, or sell any patented invention that may in any way be related thereto.

This report has been reviewed by the Information Office (OI) and is releasable to the National Technical Information Service (NTIS). At NTIS, it will be available to the general public, including foreign nations.

This technical report has been reviewed and is approved for publication.

WALTER H. REIMANN, Project Engineer

THEODORE NICHOLAS
Project Leader

NG Tupper

NATHAN G. TUPPER
Chief, Metals Behavior Branch
Metals and Ceramics Division

"If your address has changed, if you wish to be removed from our mailing list, or if the addressee is no longer employed by your organization please notify AFML/LLN *,W-PAFB, OH 45433 to help us maintain a current mailing list".*

Copies of this report should not be returned unless return is required by security considerations, contractual obligations, or notice on a specific document.

AIR FORCE/56780/23 May 1979 — 400

UNCLASSIFIED

SECURITY CLASSIFICATION OF THIS PAGE (When Data Entered)

REPORT DOCUMENTATION PAGE

READ INSTRUCTIONS BEFORE COMPLETING FORM

(14) 1. REPORT NUMBER: AFML-TR-78-159

2. GOVT ACCESSION NO.

(9) 3. RECIPIENT'S CATALOG NUMBER: Final rept.

(6) 4. TITLE (and Subtitle): THE INTERFEROMETRIC MEASUREMENT OF NEAR CRACK TIP DISPLACEMENTS IN A NICKEL BASE SUPERALLOY AT AMBIENT AND ELEVATED TEMPERATURES,

5. TYPE OF REPORT & PERIOD COVERED: Dec 1976 - April 1978

6. PERFORMING ORG. REPORT NUMBER

(10) 7. AUTHOR(s): J. Wayne Jones

8. CONTRACT OR GRANT NUMBER(s)

9. PERFORMING ORGANIZATION NAME AND ADDRESS
Air Force Materials Laboratory
Air Force Systems Command
Wright-Patterson Air Force Base, Ohio 45433

10. PROGRAM ELEMENT, PROJECT, TASK AREA & WORK UNIT NUMBERS
(16) 2307P102 (17) P1

11. CONTROLLING OFFICE NAME AND ADDRESS
Air Force Materials Laboratory (LLN)
Air Force Wright Aeronautical Laboratories (AFSC)
Wright-Patterson Air Force Base, Ohio 45433

(11) 12. REPORT DATE: March 1979

13. NUMBER OF PAGES

14. MONITORING AGENCY NAME & ADDRESS (if different from Controlling Office)
(12) 87p.

15. SECURITY CLASS. (of this report): Unclassified

15a. DECLASSIFICATION/DOWNGRADING SCHEDULE

16. DISTRIBUTION STATEMENT (of this Report)

Approved for public release; distribution unlimited.

17. DISTRIBUTION STATEMENT (of the abstract entered in Block 20, if different from Report)

18. SUPPLEMENTARY NOTES

Mr. Jones is now Assistant Professor in the Department of Materials and Metallurgical Engineering, the University of Michigan, Ann Arbor, Michigan 48109

19. KEY WORDS (Continue on reverse side if necessary and identify by block number)

Fatigue Crack Growth
Elevated Temperature
Optical Techniques

20. ABSTRACT (Continue on reverse side if necessary and identify by block number)

An optical interferometric technique is used to measure the transverse displacement field in the vicinity of the tip of a fatigue crack. The feasibility of using such a technique at temperatures as high as 732°C is demonstrated. Measurements at the crack tip indicated a region of lateral constraint which is controlled in extent by the residual deforation field surrounding the crack tip. Real-time displacement measurements provide a means of evaluating the crack closure concept and indicate that the measurement of crack opening load from →over

DD FORM 1 JAN 73 1473 EDITION OF 1 NOV 65 IS OBSOLETE

UNCLASSIFIED

SECURITY CLASSIFICATION OF THIS PAGE (When Data Entered)

012 320 4B

surface-based 'compliance' determinations leads to ambiguous results. The cyclic plastic zone within the monotonic plastic zone surrounding the crack tip is experimentally determined and compared with theory.

FOREWORD

This report describes an in-house effort conducted in the Metals Behavior Branch, Metals and Ceramics Division, Air Force Materials Laboratory, Wright-Patterson Air Force Base, Ohio. The research was conducted under Project No. 2307, "Mechanics of Materials," Task No. P1, "Life Analysis and Failure Mechanics in Engine and Airframe Structural Metals and Composites." The work reported herein was performed during the period December 1976 to April 1978, under the direction of Walter H. Reimann (AFML/LLN), project engineer. The report was released by the author in October 1978.

The author expresses his appreciation to the National Research Council which, through the award of a Postdoctoral Associateship, supported the research described in this report. The author also expresses his appreciation to the Air Force Materials Laboratory for providing the facilities. In particular the author acknowledges the assistance provided by Dr. W. H. Reimann during the course of this work. Dr. D. M. Corbly and Mr. D. E. Macha contributed greatly as co-researchers and their efforts are sincerely appreciated. The able laboratory assistance of Mr. Charles Bell and Ms. Sue McKee is appreciated. Thanks are also due to Ms. Kay Caroll who patiently typed the manuscript.

TABLE OF CONTENTS

TABLE OF CONTENTS (CONTINUED)

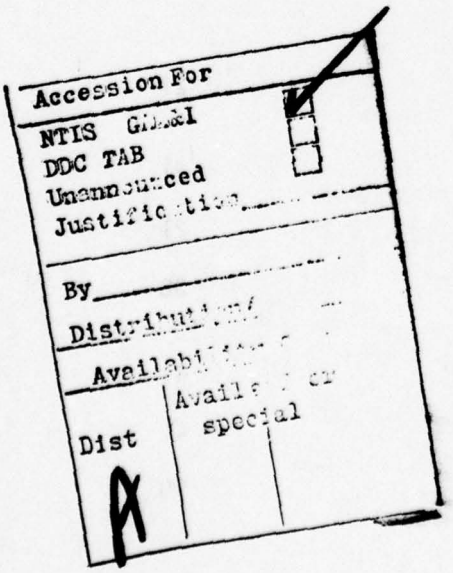

LIST OF ILLUSTRATIONS

LIST OF ILLUSTRATIONS (CONTINUED)

LIST OF ILLUSTRATIONS (CONTINUED)

LIST OF ILLUSTRATIONS (CONTINUED)

SECTION I

INTRODUCTION AND BACKGROUND

Successful prediction of usable service life of aircraft engine components depends, among other factors, on the accurate prediction of the effects of cyclic stress, temperature and aggressive gaseous environments on crack propagation behavior in engine materials. The study of crack propagation behavior under conditions which simulate actual service conditions is time consuming, expensive, and complicated by many experimental difficulties. Therefore, the common approach is to investigate the effect of a limited number of variables on crack propagation with the goal of eventual incorporation of the results into a fundamental crack propagation model which will include the important variables (and their interaction) governing crack propagation in service.

One regime of crack propagation receiving current interest is that of creep crack growth. Creep crack growth can be simply defined as the time dependent extension of a flaw experiencing a static applied stress at elevated temperatures. Early investigations into creep crack propagation (References 1,2) were able to describe the rate of crack growth in terms of the applied stress intensity factor, K, as

$$\frac{da}{dt} = AK^{\alpha} \qquad (1)$$

where A and α are constants. Similar dependencies have been observed on a variety of materials and specimen configurations (References 3-10). Comparisons of results from several of these investigations have been made by Haigh (Reference 11) and the values of α he reports from the literature range from 4.5 to 30. This range is considerably greater than that found for fatigue crack growth (Reference 12) and probably reflects the greater sensitivity of creep crack growth to factors such as crack length, specimen geometry, and stress level.

While linear elastic fracture mechanics, as implied by the use of Equation 1, may be applicable to high strength creep resistant materials, its use in general for creep crack growth prediction is suspect. In materials which undergo considerable time dependent stress relaxation in the vicinity of the crack tip the use of the stress intensity factor (which describes the stresses only in the vicinity of the crack tip) will be subject to error when different specimen geometries are considered. This has led to investigations of net section stress, crack tip opening displacement, and reference stress as parameters which might successfully describe creep crack growth.

Experimental data gathered by Nicholson and Formby (Reference 13) on the creep crack growth behavior of 316 stainless steel tested at 740°C indicate that net section stress, σ_{net}, is a better parameter for correlating crack propagation data than is stress intensity. Single edged notched specimens and notched center hole specimens were used in this study and for both geometries the crack propagation rate could be expressed as

$$\frac{da}{dt} = A\sigma_{net}^{n} \qquad (2)$$

where A and n are constants which depend on temperature.

Further studies by Nicholson (Reference 14) on 316 stainless tested at various temperatures indicated that the exponent in Equation 2 was numerically equal to the exponent in the expression for secondary creep rate given by

$$\dot{\varepsilon} = A'\sigma^{m} \qquad (3)$$

where A' and m are constants. It is possible to relate the displacement rate or crack opening rate at the crack tip to the macroscopic strain rate provided the width of the deforming crack tip region is known. If a critical crack tip opening or crack tip strain exists at which crack propagation will occur then the crack propagation rate can be related to the crack tip displacement rate. Such correlation has been found by Nicholson (Reference 14) for 316 stainless and by Haigh (Reference 15) who found creep crack growth in a range of Cr-Mo-V steels to obey the relation

$$\frac{da}{dt} = B\left(\frac{d\delta}{dt}\right)^{0.8} \tag{4}$$

where B is a constant for each steel and δ, the crack opening displacement is greater than a critical crack opening displacement as defined by Wells and McBride (Reference 16). Similar observations were made by Pilkington et al. (Reference 17) although they did not express their results in the form of Equation 3.

The crack tip failure process controls the rate of crack propagation regardless of the macroscopic parameters which appear to correlate the data. A knowledge of the failure process is important in determining the appropriate failure criterion to use in modeling creep crack propagation. Several investigations have attempted to determine crack tip failure criteria by experimental observation and theoretical prediction. A critical crack tip opening displacement has been proposed (Reference 17). Similarly, from observations on the effect of grain size on creep crack growth in nickel-base superalloys, Floreen and Kane (Reference 18) hypothesized a critical crack tip strain for creep crack propagation. Larson and Floreen (Reference 19) also explained the dependence of creep crack growth on grain morphology by a critical strain criterion.

Barnby (References 20,21) has computed the stress relaxation behavior ahead of a crack under creep conditions and has proposed that the crack tip strain controls the crack propagation rate. Vitek (Reference 22) has modeled the growth of the crack tip plastic zone in terms of a dislocation array and has shown good correlation with experiment for crack initiation time (Reference 23), and crack propagation rate.

The current state of the development of accurate failure criteria for the crack tip region depends strongly on crack tip deformation parameters which are both difficult to measure and sensitive to microstructural and geometric variables. The theory of Vitek requires a determination of the time dependent plastic zone size dimension. The strain criteria usually require a rather arbitrary selection of a critical strain value. Crack tip opening displacement can be inferred from load line displacement data in certain situations but the general validity of this approach has not been fully investigated.

Further complications arise due to the constraints imposed by specimen geometry. Gooch (Reference 24) et al. have developed a creep brittleness diagram to illustrate the role of specimen configuration and microstructure on creep crack growth. They show the importance of bending, crack length, and specimen size in determining whether creep crack growth can be described by linear elastic fracture mechanics or strain controlled parameters. Clearly, any theory which describes crack initiation and creep crack growth must take into account all such variables when choosing appropriate crack advance criteria. It is also clear that further development of accurate creep crack growth predictive capabilities depends on the development of experimental methods of determining crack tip deformation behavior at elevated temperatures. This report describes one such experimental approach to this problem.

SECTION II

OPTICAL INTERFEROMETRY AND TRANSVERSE DISPLACEMENT MEASUREMENTS

Numerous investigations have been conducted using a variety of experimental techniques to study the deformation zone surrounding a crack tip. These techniques and the results of the studies have been reviewed elsewhere (References 25, 26). The optical interferometric method used in the present investigation was chosen because of its proposed capability to make in situ measurements of crack tip deformation in the temperature regime where specimen surface degradation would severely limit the applicability of other measurement techniques. The reader is referred to Reference 27 for a detailed review of the use of optical interferometry in fracture mechanics studies at ambient temperatures.

In the present study an interference pattern was created on a transverse surface of a standard fracture mechanics specimen in which a crack was grown by fatigue. The interference pattern was produced by placing an optically flat quartz cylinder in contact with the specimen surface and illuminating the specimen in the region covered by the quartz cylinder with a collimated beam of monochromatic sodium vapor light directed normally to the transverse specimen surface. With such an arrangement a small separation between the quartz cylinder and the specimen surface causes attenuation in the intensity of the light reflected from the specimen. The degree of attenuation depends on the separation between the quartz cylinder and the specimen surface. With normal incidence maximum attenuation in air is given by

$$\Delta = \frac{1}{2}(n-1)\lambda \qquad n = 1,2,3,.... \quad \text{(Destructive Interference)} \tag{5}$$

and minimum attenuation is given by

$$\Delta = \frac{1}{2}n\lambda \qquad n = 1,2,3,.... \quad \text{(Constructive Interference)} \tag{6}$$

λ is the wavelength of the monochromatic light (λ = 0.5893 μm for sodium vapor) and n is the order of the fringes produced. Thus, changes in displacement between the quartz flat and the specimen surface can be detected by observations of the changes in the fringe patterns produced. The conditions for interference are shown diagrammatically in Figure 1.

The technique described previously is capable of accurately measuring small changes in displacement normal to the direction of viewing. For the case of crack tip, transverse displacements occur during loading as a result of Poisson contractions in the crack tip region. For very thin specimens the transverse displacements can be converted directly into transverse strain by assuming that this strain is uniform through the specimen thickness. Thus, for a specimen thickness of t and a measured contraction of δ the strain is given simply as

$$\varepsilon_z = \frac{2\delta}{t} \tag{7}$$

and the crack tip transverse strain field can be determined from the interferometrically determined transverse displacement field.

Transverse crack tip deformation at elevated temperatures can be elastic, plastic, and time dependent (deformation resulting from creep). In terms of the principal in-plane stresses the transverse elastic strain can be expressed as

$$\varepsilon_z^e = \frac{-\nu}{E} \ (\sigma_x + \sigma_y) \tag{8}$$

and the plastic transverse strain can be determined from the constancy of volume as

$$\varepsilon_z^p = - \ (\varepsilon_x^p + \varepsilon_y^p) \tag{9}$$

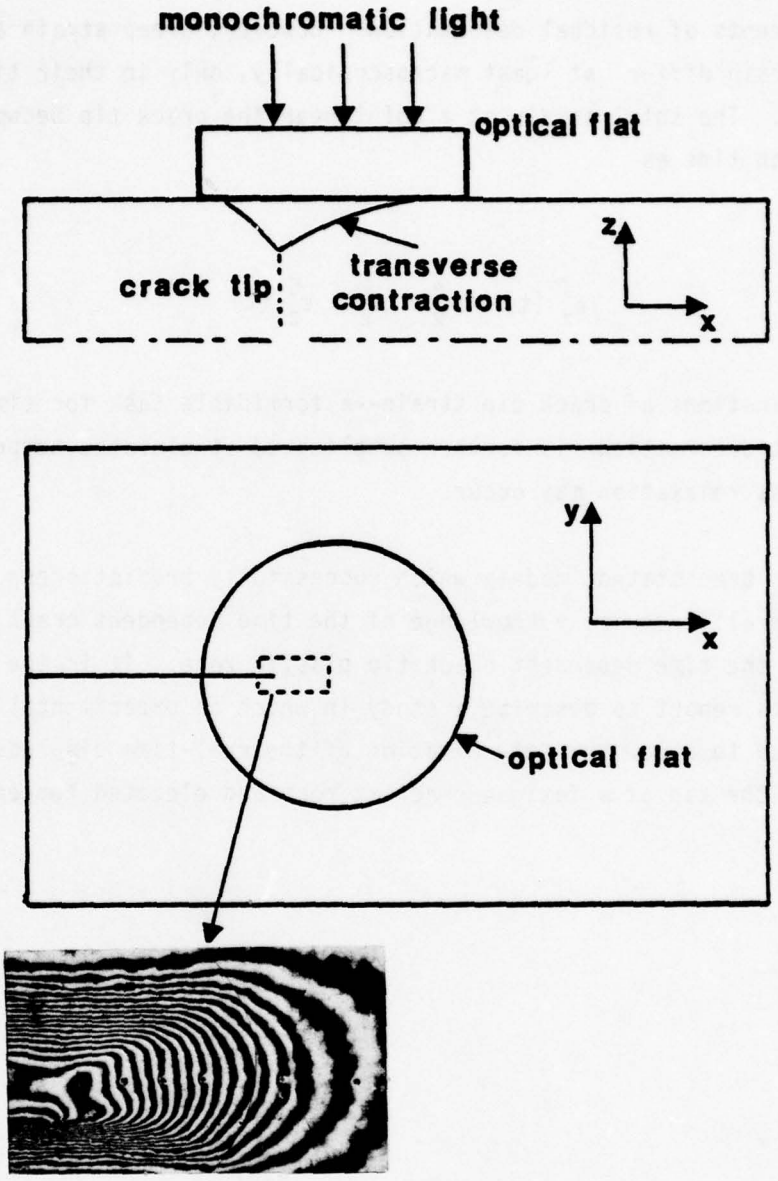

Figure 1. Illustration of the Physical Conditions on the Specimen Surface Required to Produce an Interference Pattern. The Magnitude of Deformation Shown Is Greatly Exaggerated for Clarity.

Elastic strain can be distinguished experimentally from plastic strain by measurements of residual deformation. However, creep strain and plastic strain differ, at least macroscopically, only in their time dependence. The total strain at a point near the crack tip becomes dependent on time as

$$\varepsilon_z^T(t) = \varepsilon_z^e + \varepsilon_z^P + \varepsilon_z^C(t) \tag{10}$$

The determinations of crack tip strain--a formidable task for time independent deformation--is further complicated at elevated temperatures where stress relaxation may occur.

As has been stated, models which successfully predict creep crack growth generally require a knowledge of the time dependent crack tip strain and the time dependent crack tip plastic zone. It is the purpose of this report to describe a study in which an experimental technique is developed to allow the determination of the real-time displacement changes at the tip of a fatigue crack at room and elevated temperatures.

SECTION III

EXPERIMENTAL DETAILS

1. MATERIAL

The material chosen for this study was Gatorized™ IN-100, a nickel base superalloy used in aircraft turbine applications. The nominal mechanical properties of this alloy for the temperature range of interest are given in Table 1.

2. SPECIMEN CONFIGURATION

All specimens studied were of the modified compact configuration (H/W = 0.486) as shown in Figure 2. The stress intensity factor for this configuration was computed from

$$K = \frac{P\sqrt{a}Y}{BW} \qquad (11)$$

where P is the applied load, B is specimen thickness, W is specimen width and Y is a geometric calibration factor given by

$$Y = 30.96 - 195.8(a/W) + 730.6(a/W)^2 - 1186.3(a/W)^3 + 754.6(a/W)^4 \qquad (12)$$

3. FATIGUE CRACK GROWTH

Fatigue crack growth was conducted in a closed loop servo-hydraulic testing machine operating at a cyclic frequency of 20 hz. The maximum stress intensity, K_{max}, was held constant during crack growth at 38.5 MPa $\sqrt{m}$ (35 ksi $\sqrt{in}$) by standard load shedding techniques. The minimum stress intensity, K_{min}, was adjusted to keep the ratio K_{min}/K_{max} constant

TABLE 1

MECHANICAL PROPERTIES OF GATORIZED^{TM} IN-100

Temp. (^{o}C)	Modulus (MN/m^2)	Mean Yield Stress (MN/m^2)
25	214 x 10^3	1.12 x 10^3
100	210	1.11
300	200	1.07
500	189	1.09
750	172	1.08

at a value of 0.1. All crack length measurements were made at the specimen surface using Gaertner travelling microscopes. Crack lengths reported are the averages of measurements from both specimen surfaces. At preselected crack lengths the specimens were removed from the servo-hydraulic testing machines. Fiducial markings were placed in the crack tip region and the specimens were placed in a screw driven testing machine for room temperature displacement studies or returned to the servo-hydraulic testing machine for measurements at elevated temperatures.

4. SPECIMEN SURFACE PREPARATION

Specimen surfaces to be studied were machined to nominal flatness during the course of specimen fabrication. Further preparation included manual wet grinding through a series of decreasing grit sizes followed by lapping with diamond paste. This assured a flat surface relatively free of scratches. In most cases specimens were preoxidized below the temperature at which they were to be tested. Room temperature specimens were also preoxidized since it was found that preoxidizing reduced the surface reflectivity which improved fringe contrast.

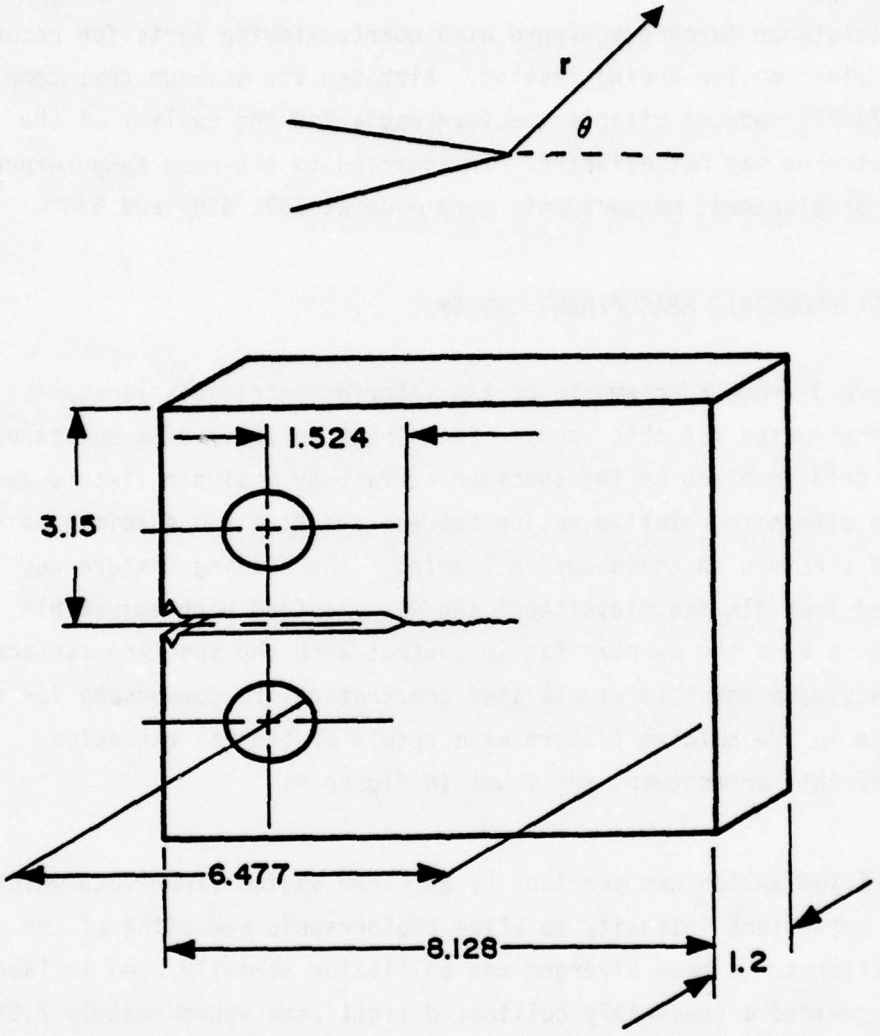

Figure 2. Test Specimen Configuration and Dimensions (cm). Inset Indicates Coordinate System Used in this Study.

5. ELEVATED TEMPERATURE TESTING

Heating of the specimens for the elevated tests was accomplished with a resistance furnace equipped with quartz viewing ports for recording the fringe motion during testing. Although the maximum test temperature of 732°C produced visible specimen radiation the quality of the fringe patterns was not affected. In addition to the room temperature studies, displacement measurements were made at 732, 650, and 538°C.

6. INTERFEROMETRIC MEASUREMENT SYSTEM

Figure 3 shows a schematic of the interferometric displacement system constructed for this study. The system consists of a quartz optical flat held in place on the specimen surface by a simple fixture designed to eliminate relative motion between the flat and specimen as a result of specimen rotation during loading. The holding fixture was fabricated from 316 stainless steel and was provided with adjustable screws which kept the quartz flat in contact with the specimen surface. Adjustments were possible at elevated temperatures to compensate for the distortion in the holding fixture as a result of thermal expansion. Details of this arrangement are shown in Figure 4.

The illumination was provided by an Osram sodium vapor lamp which provided sufficient intensity to allow photographic recording of the fringe patterns. A beam diverger and collimator normally used in laser systems provided a reasonably collimated light beam approximately 2.54 cm (1.0 in) in diameter. This was more than sufficient to cover the specimen area under investigation. A quartz cube beam splitter was used to allow illumination and viewing normal to the specimen surface.

The crack tip region was observed through a travelling microscope with a working distance of approximately 18 cm. Fringe patterns at the crack tip were either observed directly through the microscope,

recorded on 35 mm film with a camera attached to the microscope or recorded on video tape. The latter approach used a standard video camera positioned behind the microscope. With the lens removed from the camera the image from the microscope was focused directly onto the video photo sensor. A relatively broad range of magnifications could be obtained with the microscope-video camera arrangement simply by positioning the microscope and camera at various distances from the specimen surface.

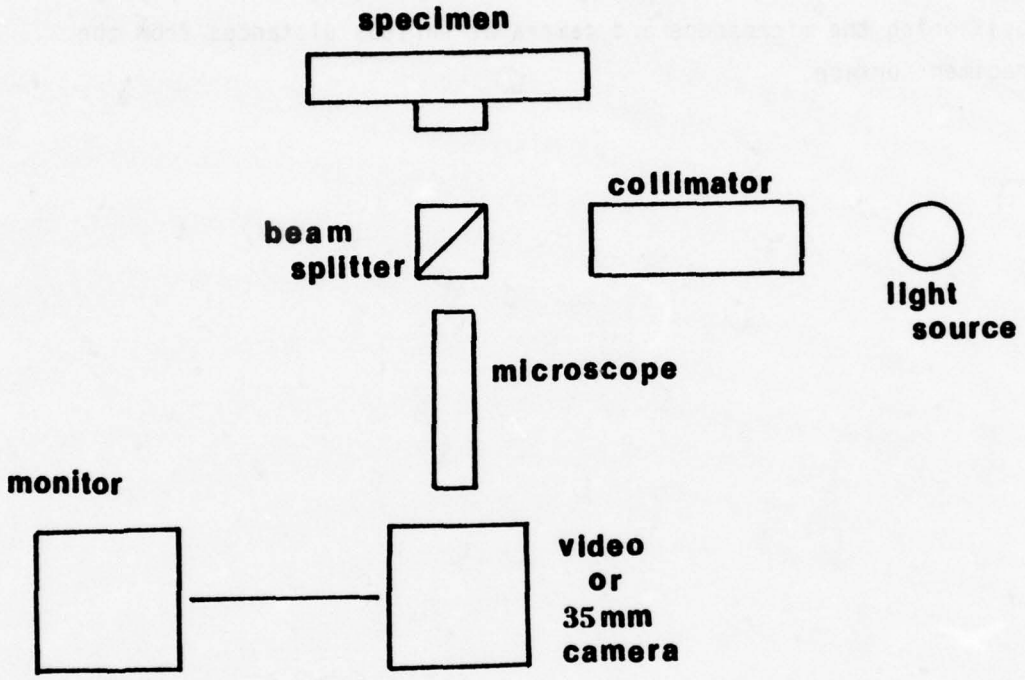

Figure 3. Schematic of Interference Displacement Measurement System. For Elevated Temperature Testing the Specimen Is Enclosed in a Resistance Furnace Equipped with Quartz Windows.

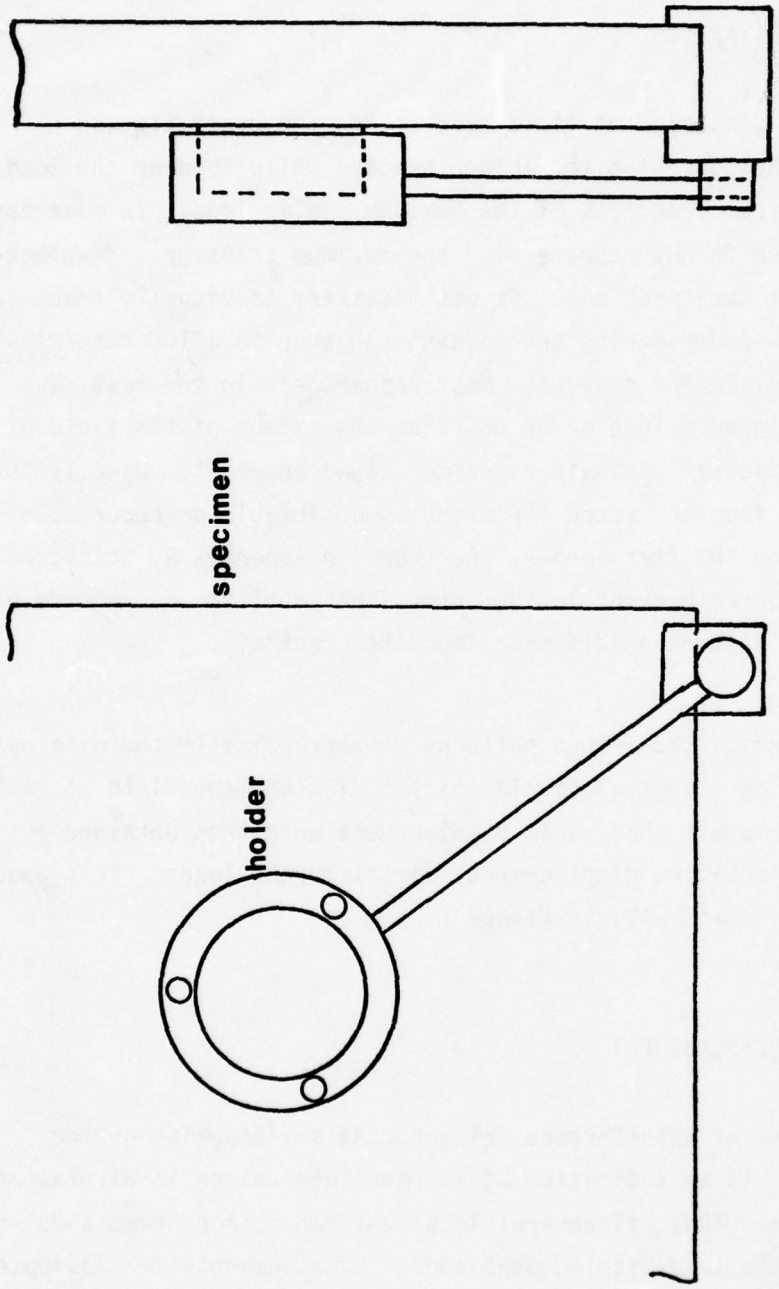

Figure 4. Illustration of Optical Flat Holder Used for Ambient and Elevated Temperature Testing

SECTION IV

PROCEDURES FOR DISPLACEMENT MEASUREMENTS

1. DISPLACEMENT FIELD

The entire displacement field surrounding the crack tip was determined by photographing the fringe pattern while holding the load constant at various fractions of the maximum cyclic load. In most cases the highest order fringe representing the maximum transverse displacement occurred at the crack tip. It was necessary to visually track the change in fringe order during the loading sequence to allow determination of absolute displacement changes. Most researchers in the past have arbitrarily assigned fringe order based on the extent of the field of observation particular to their experimental arrangement. Usually the farthest fringe from the crack tip which is observable or recordable has been assigned the first order. As shown in Appendix A, this can result in considerable error in the determination of the dependence of transverse displacement on distance from the crack tip.

After recording the fringe patterns photographically the data was digitized to allow graphical display of the displacement field at each load tested. Absolute changes in displacement were then obtained by subtracting the relative displacements for different loads. This procedure is shown schematically in Figure 5.

2. REAL-TIME DISPLACEMENT

The movement of interference fringes past any location on the specimen surface is an indication of the absolute change in displacement at that location. Thus, if several locations can be monitored simultaneously then the load-displacement and/or displacement-time response can be determined as a function of location with respect to the crack tip. The following procedure was devised to make such measurements.

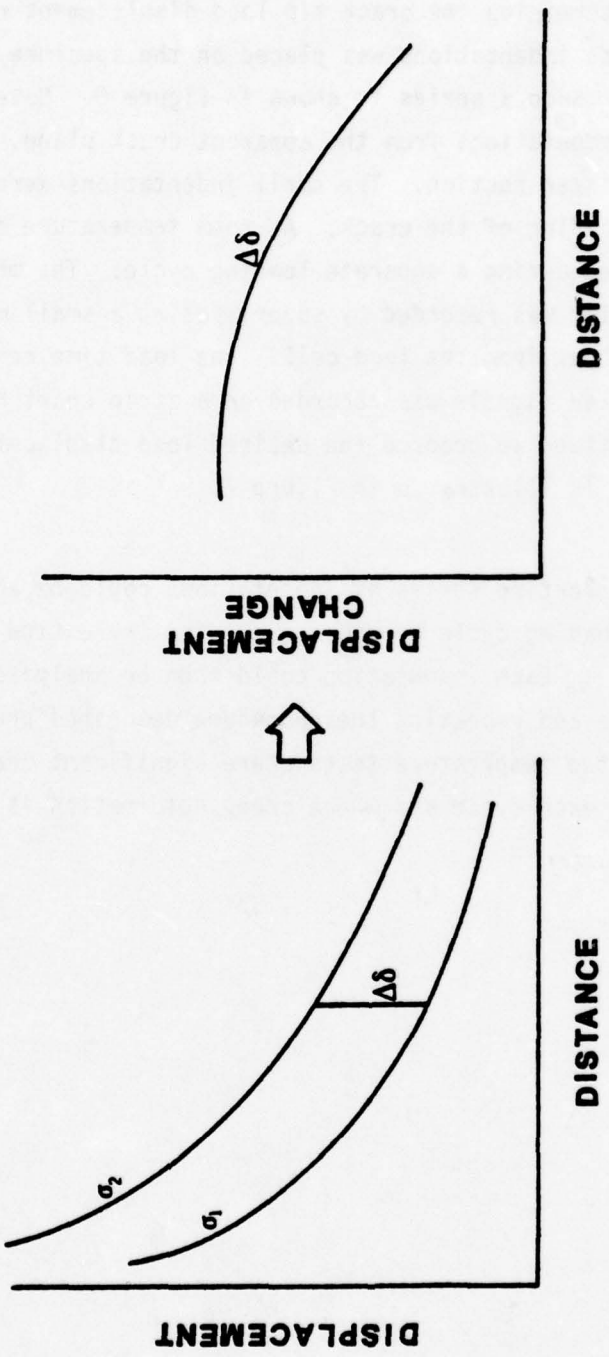

Figure 5. Diagrammatic Representation of Method Used to Obtain Absolute Displacement Data. Fringe Motion Must Be Monitored Visually During Loading.

For the case of determining the crack tip load displacement response a series of microhardness indentations was placed on the specimen surface ahead of the crack tip. Such a series is shown in Figure 6. Note, the offset of the line of indentations from the apparent crack plane. This will be discussed in a later section. The small indentations were monitored visually during loading of the crack. At room temperature each indentation was monitored during a separate loading cycle. The motion of fringes past each point was recorded by superimposing a small marker signal on the analog output from the load cell. The load time response together with these marker signals was recorded on a strip chart recorder. The data were then digitized to produce the desired load displacement record. This procedure is illustrated in Figure 7.

An analysis for the entire series of indentations could be accomplished with only one loading cycle by video recording the entire fringe pattern during the cycle. Each indentation could then be analyzed by replaying the video tape and repeating the procedure described previously. This is useful in elevated temperature tests where significant crack growth may occur during each cycle and where creep deformation is expected.

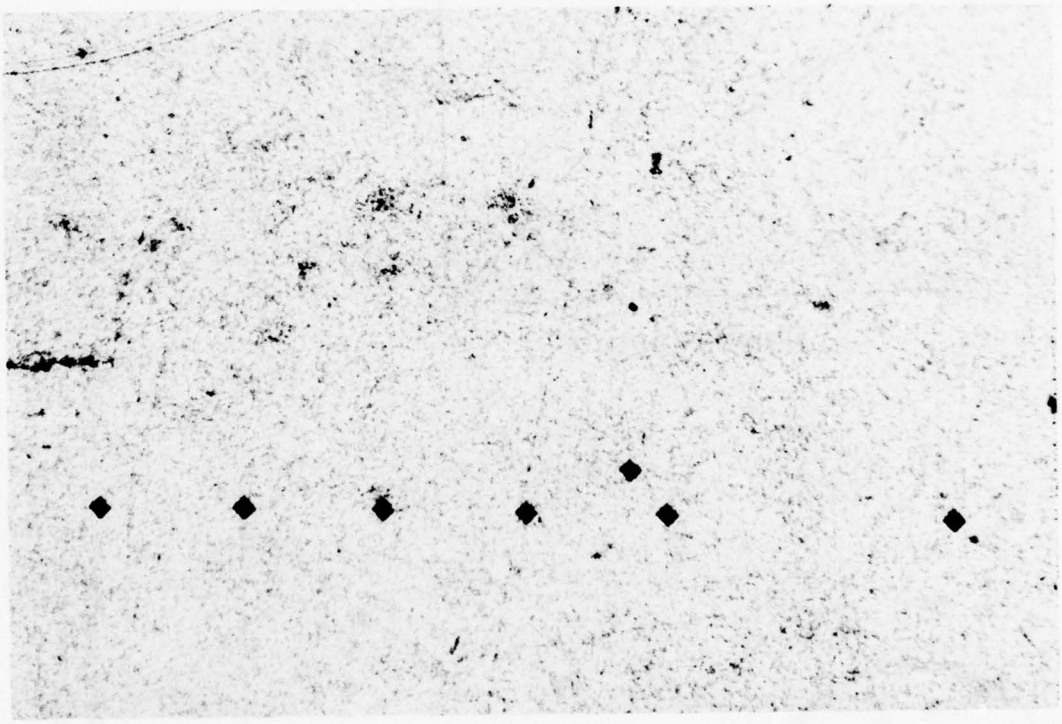

Figure 6. Typical Crack Tip Region Showing Placement of Microindentations. Indentations Are Placed Along the Line of Symmetry of the Deformation Field.

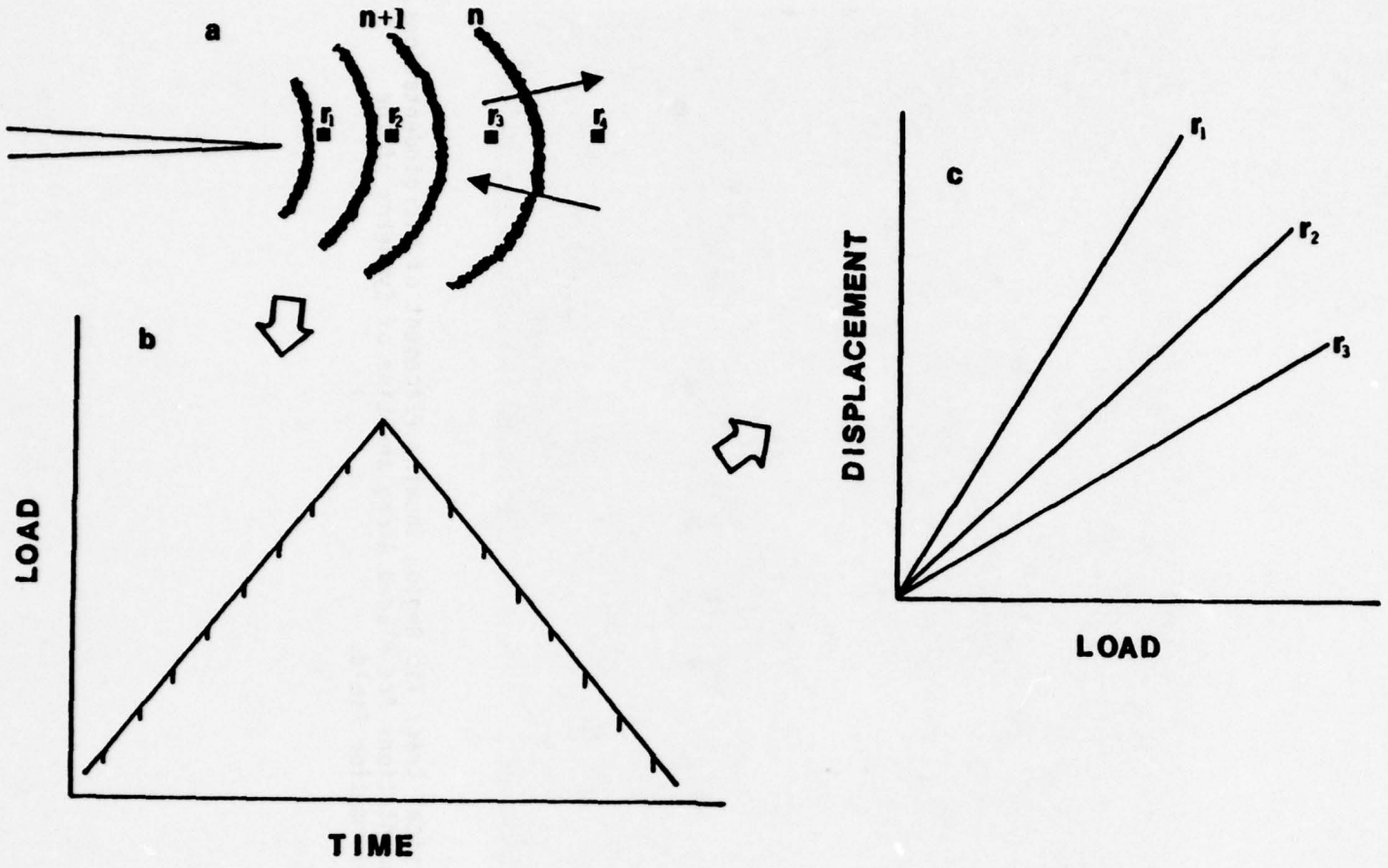

Figure 7. Diagrammatic Representation of the Method Used to Obtain Real-Time Displacement Data. In b the Mark on the Load-Time Trace Represents the Passage of a Fringe Over the Point of Observation.

SECTION V

RESULTS AND DISCUSSION

The data presented in this section are typical of all data gathered during the experimental program. The results obtained from transverse displacement measurements in the vicinity of the crack tip will be shown as a function of applied stress intensity and distance from the crack tip, r. In addition, displacement vs. applied stress intensity data from the real-time measurements of transverse displacement will be presented. Data will be presented which illustrates the use of these techniques at ambient and elevated temperatures as high as 732°C.

1. TRANSVERSE DISPLACEMENT PROFILES

a. Ambient Temperature

Figure 8 illustrates the typical interferometric patterns produced in the vicinity of the crack tip during a series of increasing applied stress intensity, K. The crack tip is denoted by the arrow and the intersection of the crack with the specimen surface is indicated by the solid line, as shown in Figure 8a. Several features common to all interface patterns observed bear mentioning. In the region surrounding the crack tip and along the crack line a region of residual deformation is observed. The cracks studied were grown under constant K_{max} and as expected the width of the deformation zone is independent of location along the crack line. The deformation zone is not symmetric about the surface crack. The line of symmetry of the elastic deformations ahead of the crack was not coincident with the projection of the crack line on the specimen surface but was shifted slightly above or below this crack line. This results from the slant fracture which occurs near the free surface of the specimen causing the crack plane near the surface to deviate from the crack plane in the interior of the specimen.

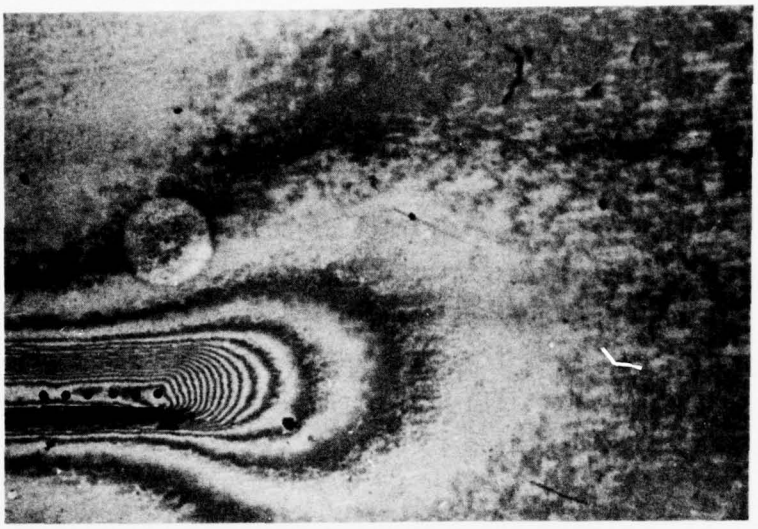

(a) $K = 7.30 \times 10^3$ MN/m$^{3/2}$

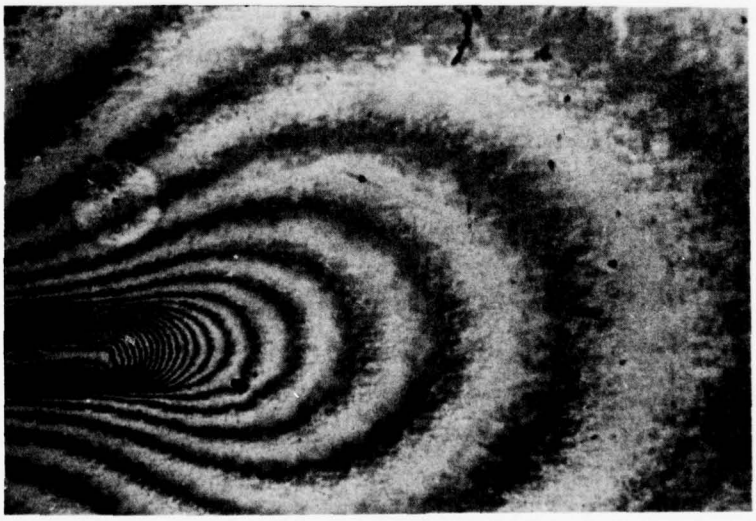

(b) $K = 16.9 \times 10^3$ MN/m$^{3/2}$

Figure 8. Interference Patterns Produced in the Crack Tip Vicinity During a Typical Load Excursion.

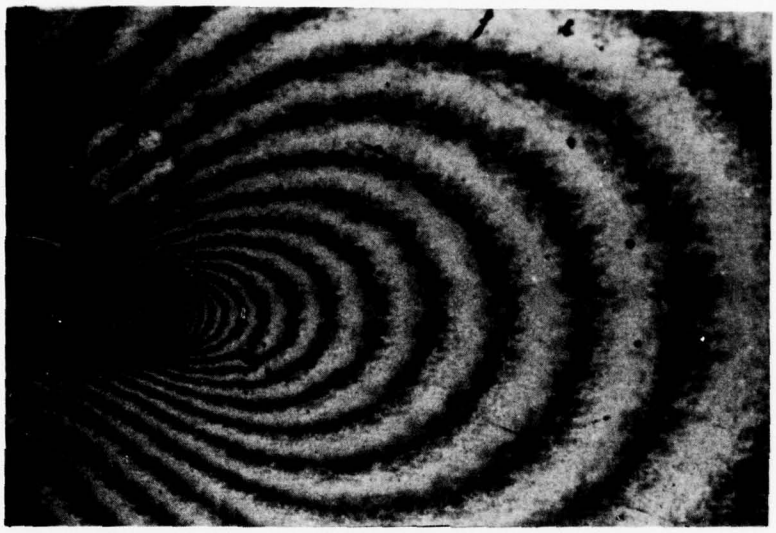

(c) $K = 3.17 \times 10^3$ MN/m$^{3/2}$

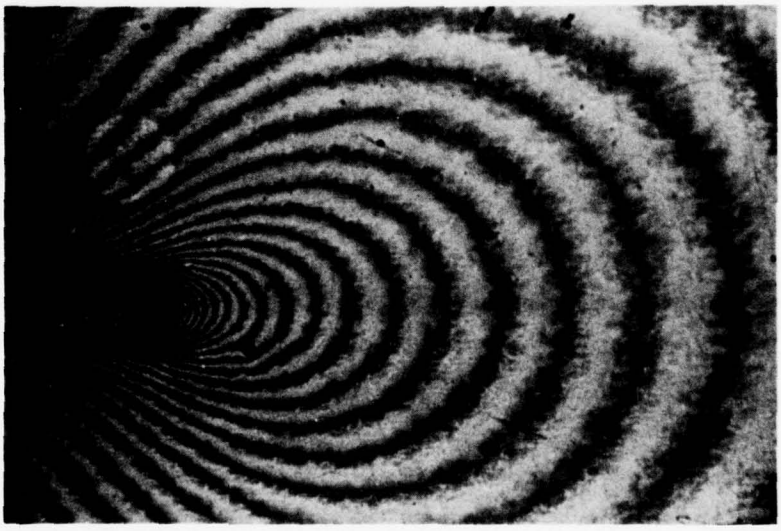

(d) $K = 37.5 \times 10^3$ MN/m$^{3/2}$

It must be assumed from this that the transverse deformation field is strongly influenced by the interior flat region of the crack. This is further illustrated in Figure 9 which is a plot of the residual transverse displacement, δ, along a direction normal to the crack propagation direction. The maximum residual deformation occurs along the line of symmetry of the previously mentioned elastic deformation field and not at the intersection of the crack with the specimen surface.

Finally, the elastic deformation field resulting from the applied stress intensity can be followed conveniently by reference to the interference patterns in Figure 8. At low stress intensity the fringe density ahead of the crack tip is very low. As the stress intensity increases the fringe density also increases indicating an increase in the transverse contraction of the specimen in the crack tip region. Reducing the stress intensity to its original value will cause the fringe pattern to assume its original configuration indicating elastic deformation surrounding the crack tip.

Typical displacement data derived from interference patterns is shown in Figure 10 for three different directions from the crack tip: along the direction of crack propagation at 45 and 90° to the direction of the crack propagation. Each of these plots shows two distinct regions of deformation behavior. Near the crack tip the deformation gradient is quite steep. Farther from the crack tip the change in displacement with distance from the crack tip is more gradual. The steeper profile at 90° to the crack plane reflects the residual deformation field shown in Figure 9.

Using the procedure outlined in Section IV, the absolute displacement as a function of stress intensity and distance from the crack tip

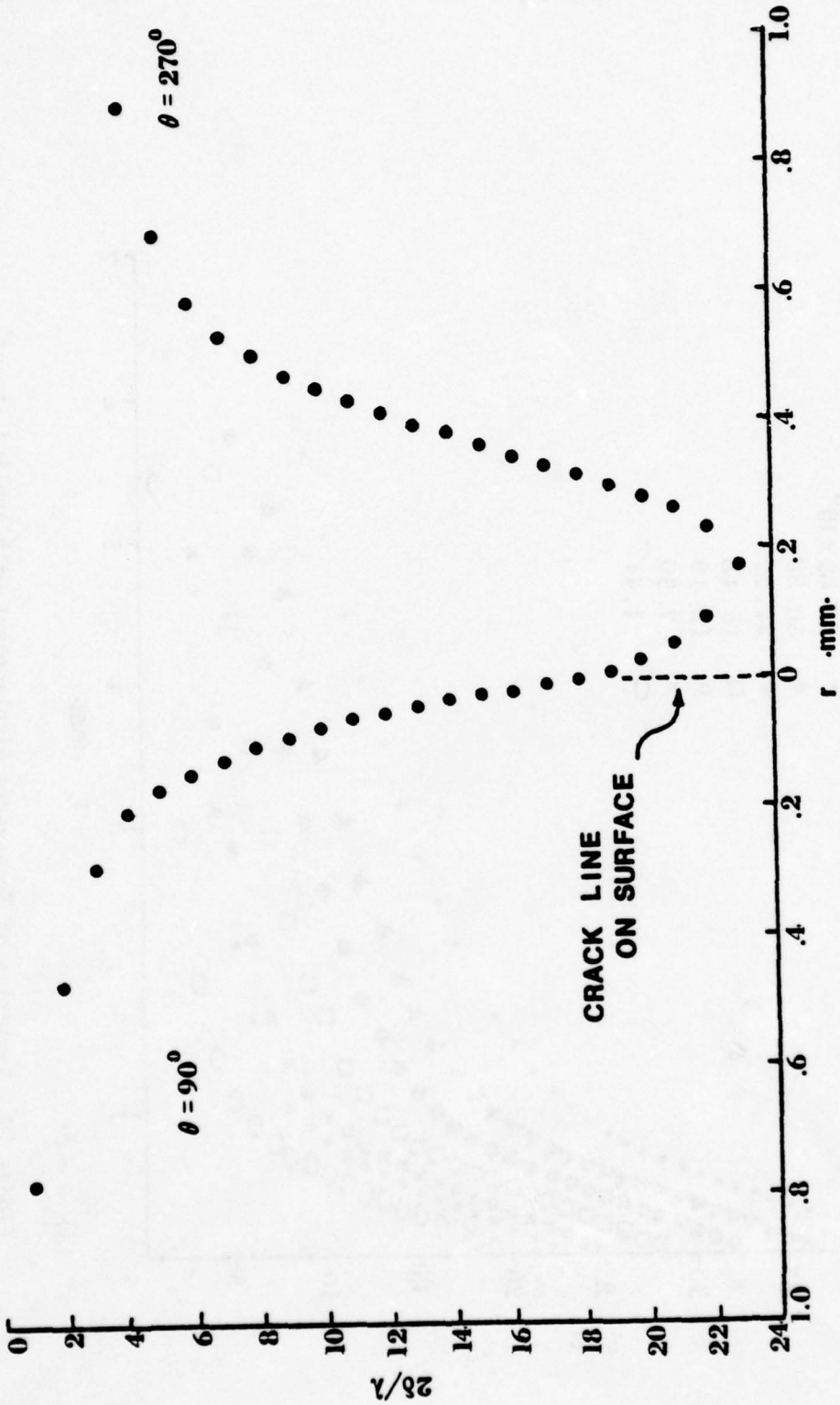

Figure 9. Transverse Displacement Variation on a Line Normal to the Crack Propagation Direction and Intersecting the Crack Line.

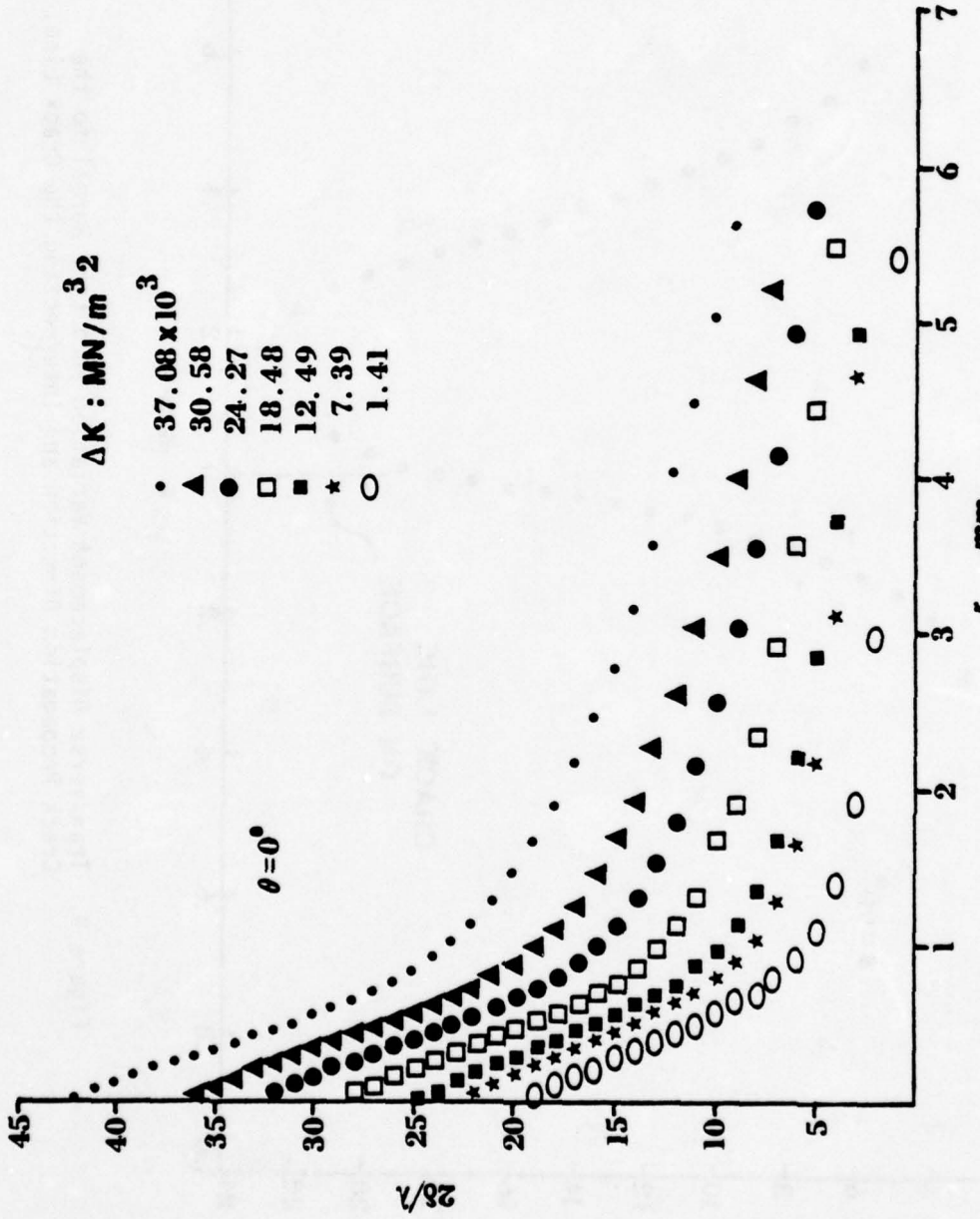

Figure 10. Variation of Transverse Displacement with Applied Stress Intensity and Distance from the Crack Tip for a Crack Length of 48.3 mm. (a) $\theta = 0°$, (b) $\theta = 45°$, (c) $\theta = 90°$

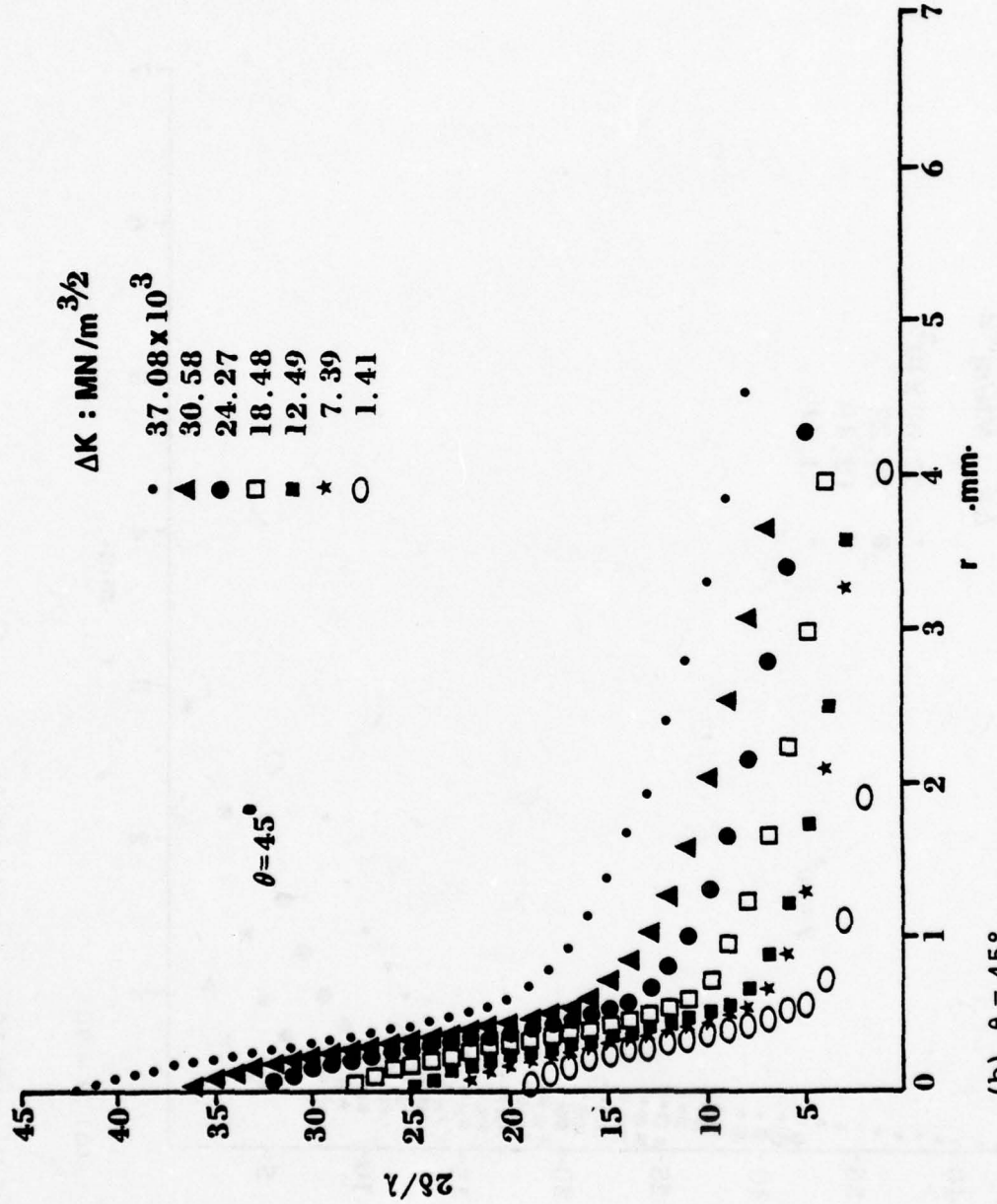

(b) $\theta = 45°$

Figure 10. (continued)

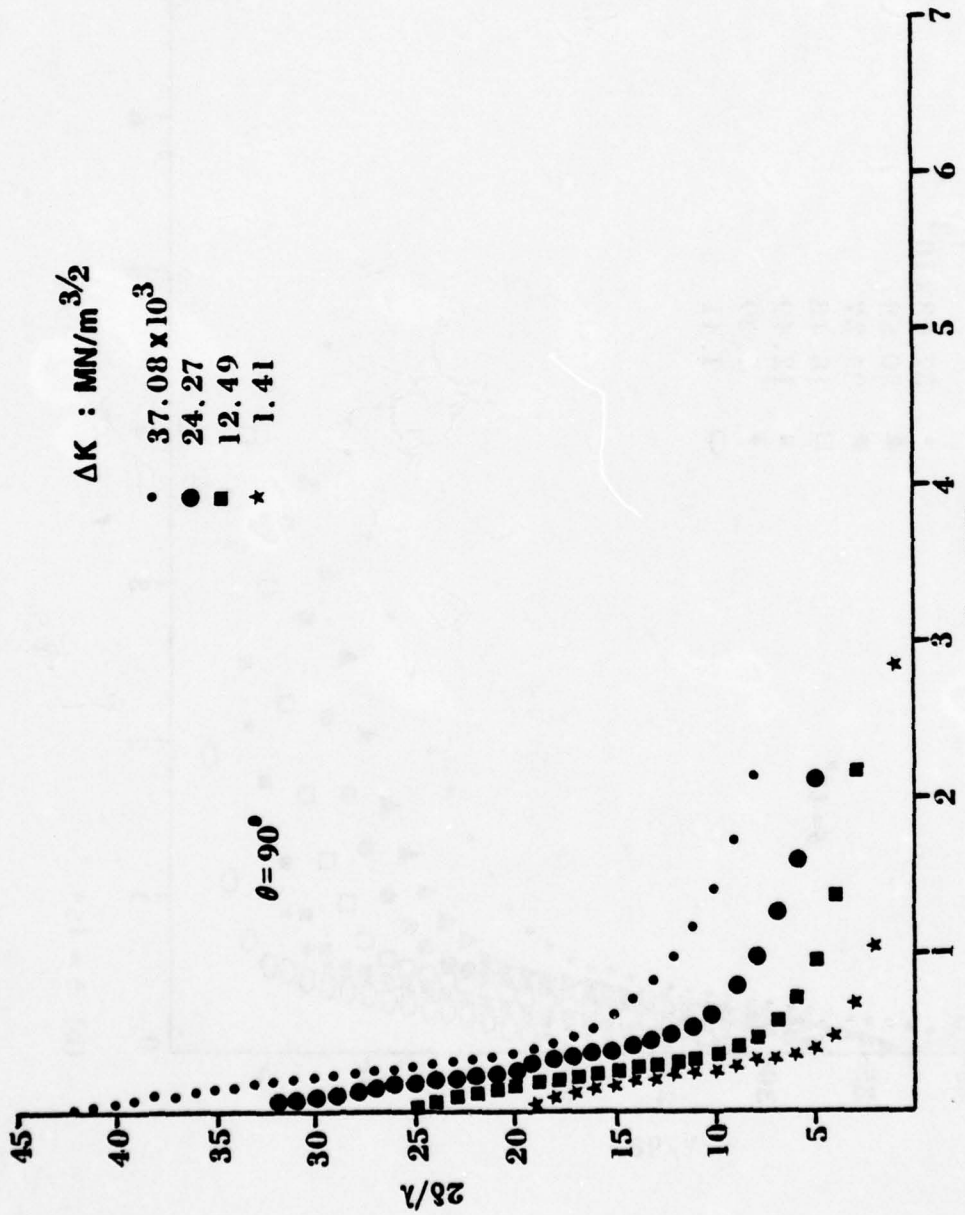

(c) θ = 90°

Figure 10. (continued)

was determined. In this report, data along the crack line will be presented for illustration. Figure 11 is a plot of the change in transverse displacement as a function of stress intensity and distance from the crack tip. Four crack lengths are represented in Figures 11a through 11d. In each figure the variation of displacement with applied stress intensity is shown as a series of roughly parallel curves.

Each curve can conveniently be divided into two distinct regions. In Region I the absolute displacement is only weakly dependent on distance from the crack tip. In Region II a strong dependence of distance from the crack tip is observed. Region I is undoubtedly the result of the constraining action of the undeformed elastic matrix on the plastic deformation field surrounding the crack tip. In the region of the residual deformation transverse stresses caused by the geometry change resulting from plastic deformation may override the effect of in-plane stresses on transverse displacements. The residual transverse displacement field for the specimen in question is shown in Figure 12. The transverse displacement profile along the crack line is shown in Figure 13. From Figures 12 and 13 it is reasonable to conclude that the extent of the residual deformation field lies between 1.0 and 1.2 mm. Reference to Figure 11 indicates that Region I for most of the curves show ends at approximately 1.0 to 1.25 mm from the crack tip. Thus, the agreement between the region of constrained transverse deformation and the region of residual transverse deformation appears to be quite good.

Linear elastic fracture mechanics predicts that to a first approximation the in-plane stresses near the crack tip vary as $1/\sqrt{r}$. From the discussion in Section III it follows that the elastic transverse displacements should also vary in this manner. The data in Region II of the absolute transverse displacement change versus distance from the

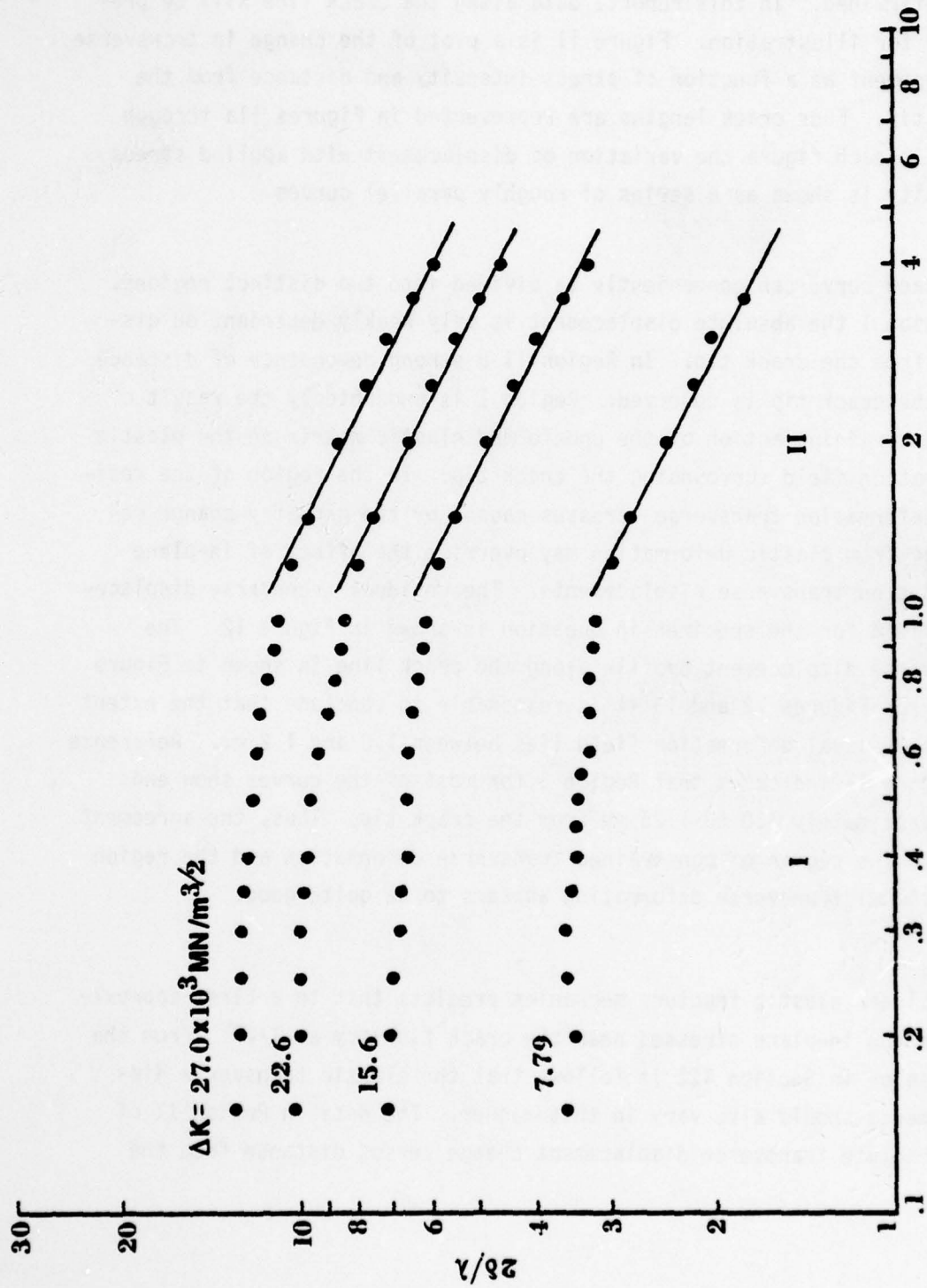

(a) a = 32.9 mm

Figure 11. Variation of Absolute Change in Transverse Displacement with Applied Stress Intensity and Distance from the Crack Tip (θ = 0°). (a) a = 32.9 mm, (b) a = 38.07 mm (c) a = 43.1 mm, (d) a = 48.3 mm

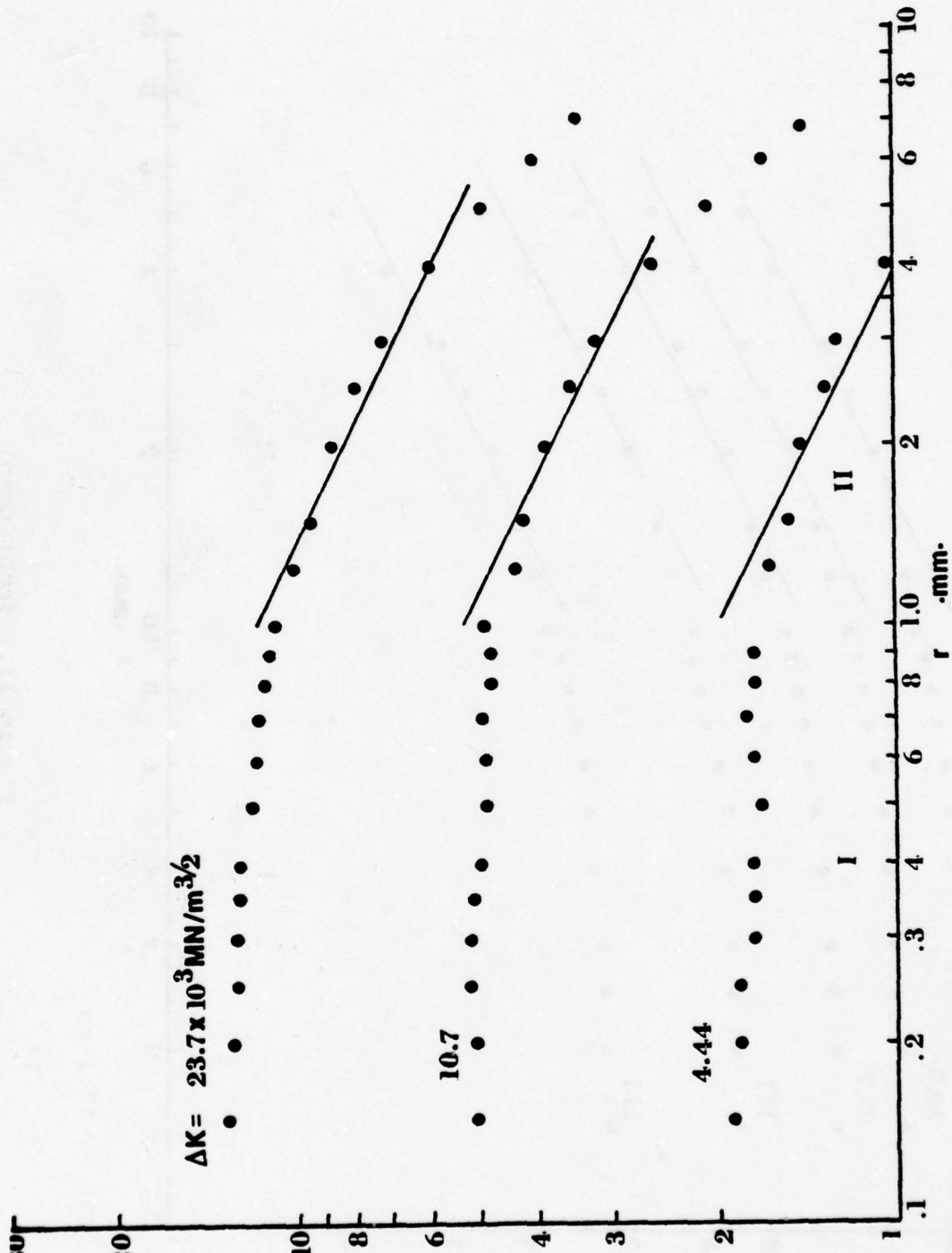

(b) a = 38.07 mm

Figure 11. (continued)

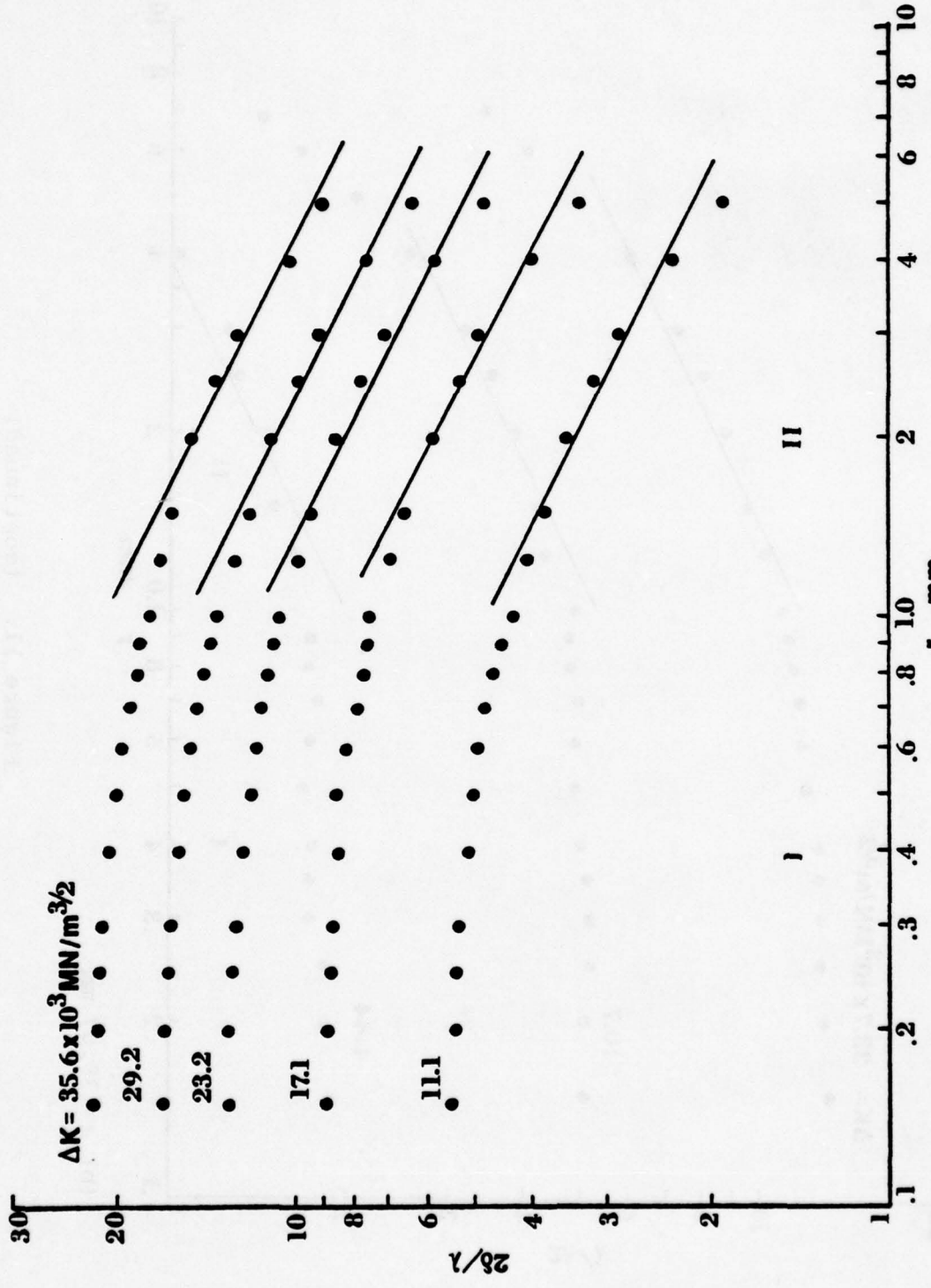

(c) a = 43.1 mm

Figure 11. (continued)

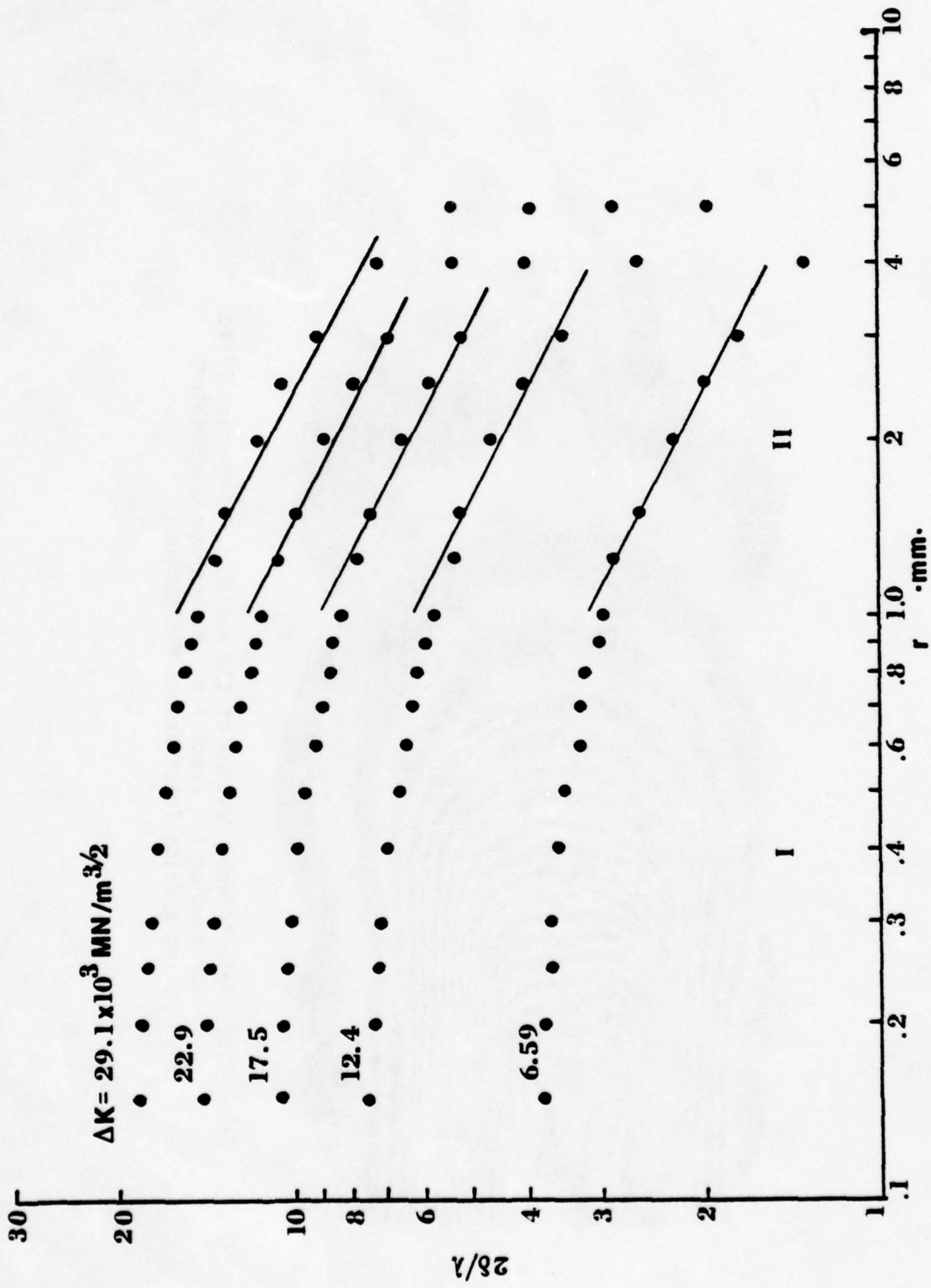

(d) a = 48.3 mm

Figure 11. (continued)

Figure 12. Interference Pattern of the Residual Deformation Field Surrounding the Crack Tip. Micrograph Was Obtained Using a Zeiss Interference Microscope

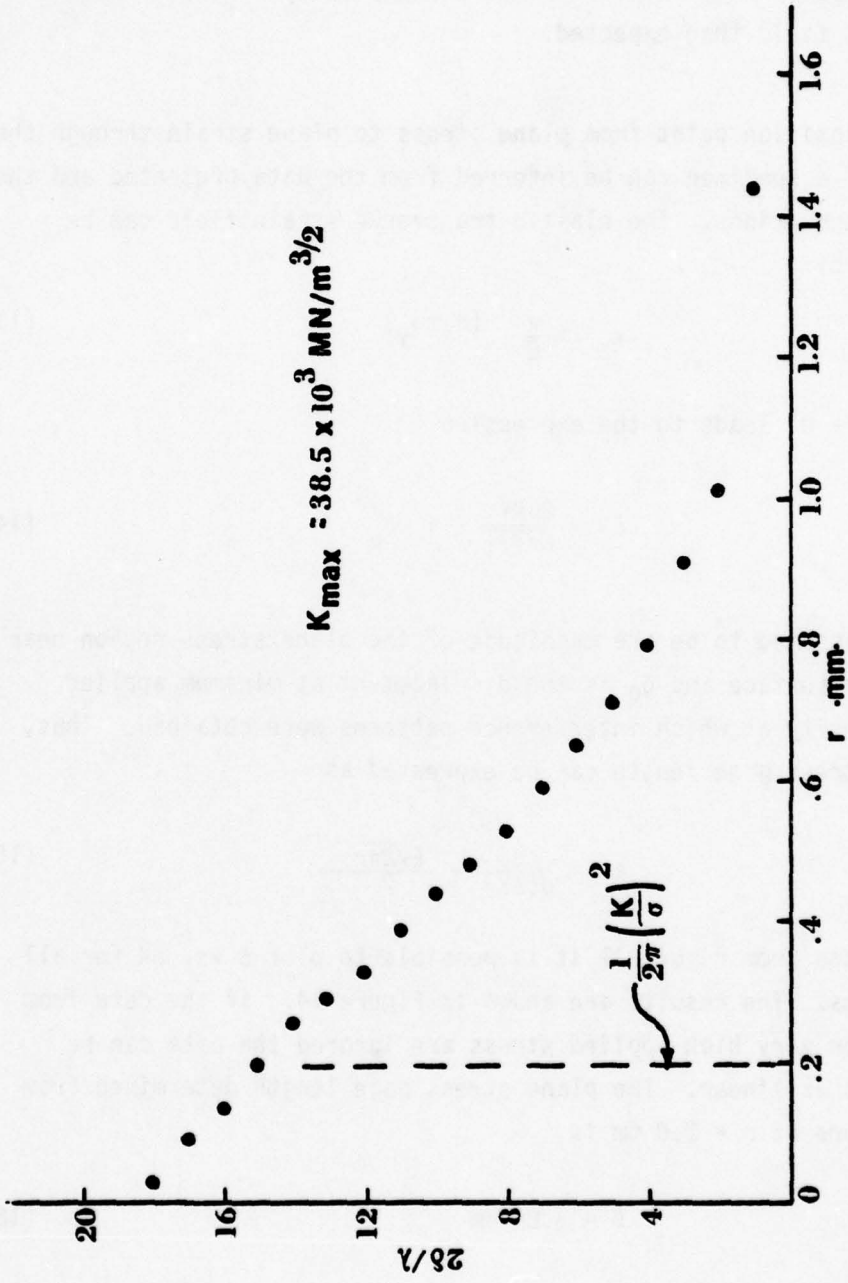

Figure 13. Variation of the Transverse Displacement for θ = 0° in Figure 12

crack tip can be approximated by a line of slope $d\delta/dr = -0.5$. At distances greater than 5 mm this dependence is not observed and steeper slopes are found which indicates a more rapid decay of the transverse displacement field than expected.

The transition point from plane stress to plane strain through the thickness of a specimen can be inferred from the data presented and the following assumptions. The elastic transverse strain field can be represented by

$$\varepsilon_z = \frac{\nu}{E} (\sigma_x + \sigma_y) \tag{13}$$

which for $\theta = 0°$ leads to the expression

$$\delta = \frac{2\nu K \ell}{E\sqrt{2\pi r}} + \delta_o \tag{14}$$

where ℓ is assumed to be the magnitude of the plane stress region near the specimen surface and δ_o is the displacement at minimum applied stress intensity at which interference patterns were obtained. Thus, the plane stress gage length can be expressed as

$$\ell = \frac{d\delta}{d(\Delta K)} \frac{E\sqrt{2\pi r}}{2\nu} \tag{15}$$

Using the data from Figure 11 it is possible to plot δ vs. ΔK for all crack lengths. The results are shown in Figure 14. If the data from the cases for very high applied stress are ignored the data can be approximated as linear. The plane stress gage length determined from this procedure at $r = 2.0$ mm is

$$\ell = 3.84 \text{ mm} \tag{16}$$

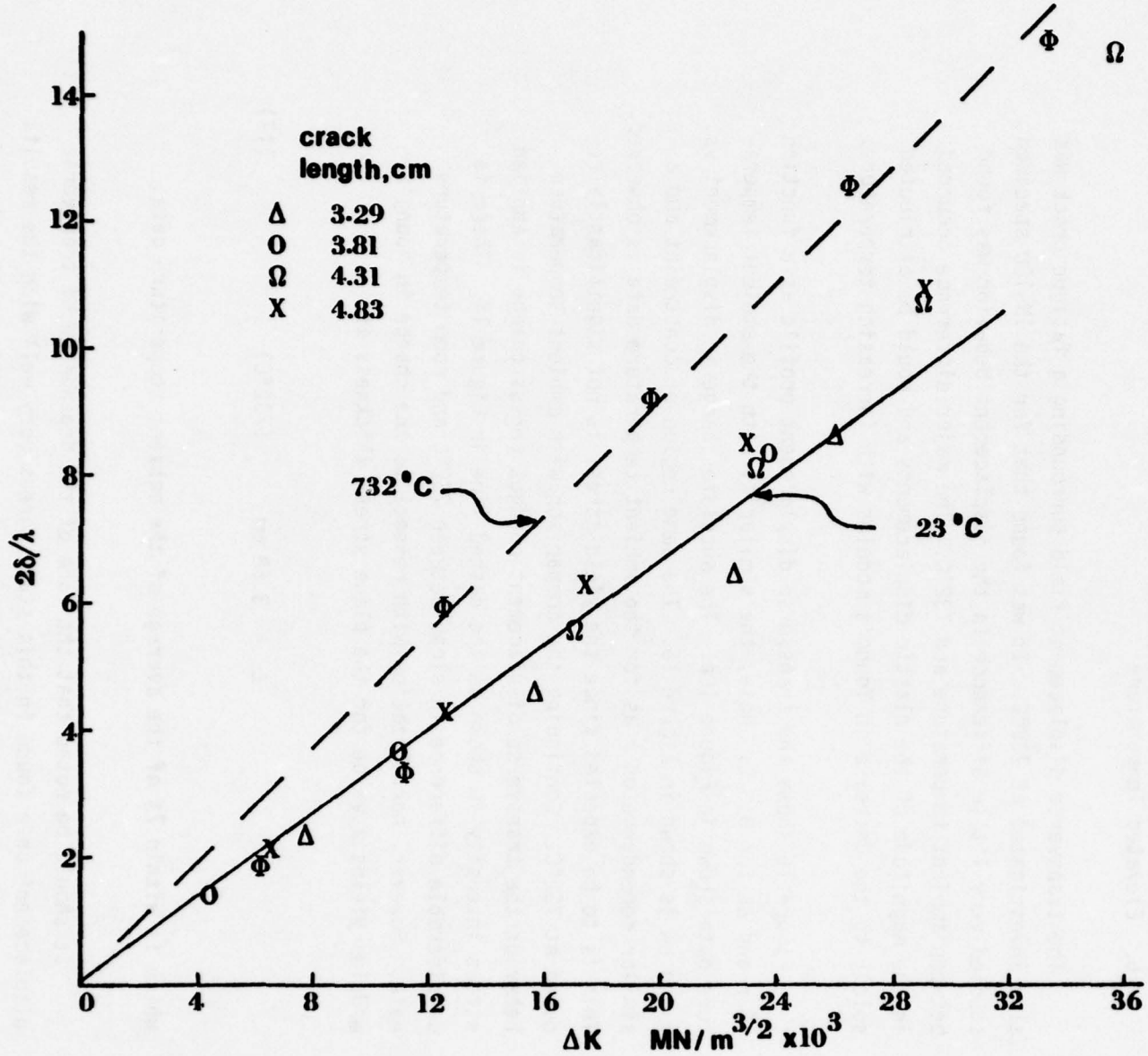

Figure 14. Change in Transverse Displacement at r = 2.0 mm with Applied Stress Intensity and Crack Length.

For the specimen thickness of 12.5 mm the plane stress region on both specimen surfaces comprises approximately 60% of the specimen thickness.

b. Elevated Temperature

The transverse displacement field surrounding a fatigue crack was also investigated at 732°C. It was found that for the IN-100 specimen studied very little difference in the displacement behavior was found between ambient temperature and 732°C. The major difference occurred in the magnitude of the elastic displacements and could be attributed solely to the decrease in Young's modulus with increasing temperature.

Figure 15 shows the transverse displacement profile as a function of r and ΔK for $\theta = 0$. Note, the similarity with the ambient temperature data shown in Figure 10a. The absolute change in displacement vs. r and ΔK is shown in Figure 16. The same region of constraint and a similar dependence on r as for the ambient temperature data is observed. This is to be expected since the yield stress is not significantly reduced at 732°C. Continuing the comparison with ambient temperature behavior the transverse displacement changes versus change in applied stress intensity is shown as the dashed line in Figure 14. There is considerable difference in slope between 732°C and room temperature data. However, normalization with respect to the change in Young's modulus yields a value for the plane stress thickness as

$$\ell = 3.58 \text{ mm} \qquad (732°C) \qquad (17)$$

which is within 7% of the average of the ambient temperature data.

It should be noted that the form of the dependence of transverse displacement on r found in this study agrees very well with the results of other investigators. Constraint near the crack tip was noted by Ke and Liu (Reference 28) and by Underwood and Kendall (Reference 29).

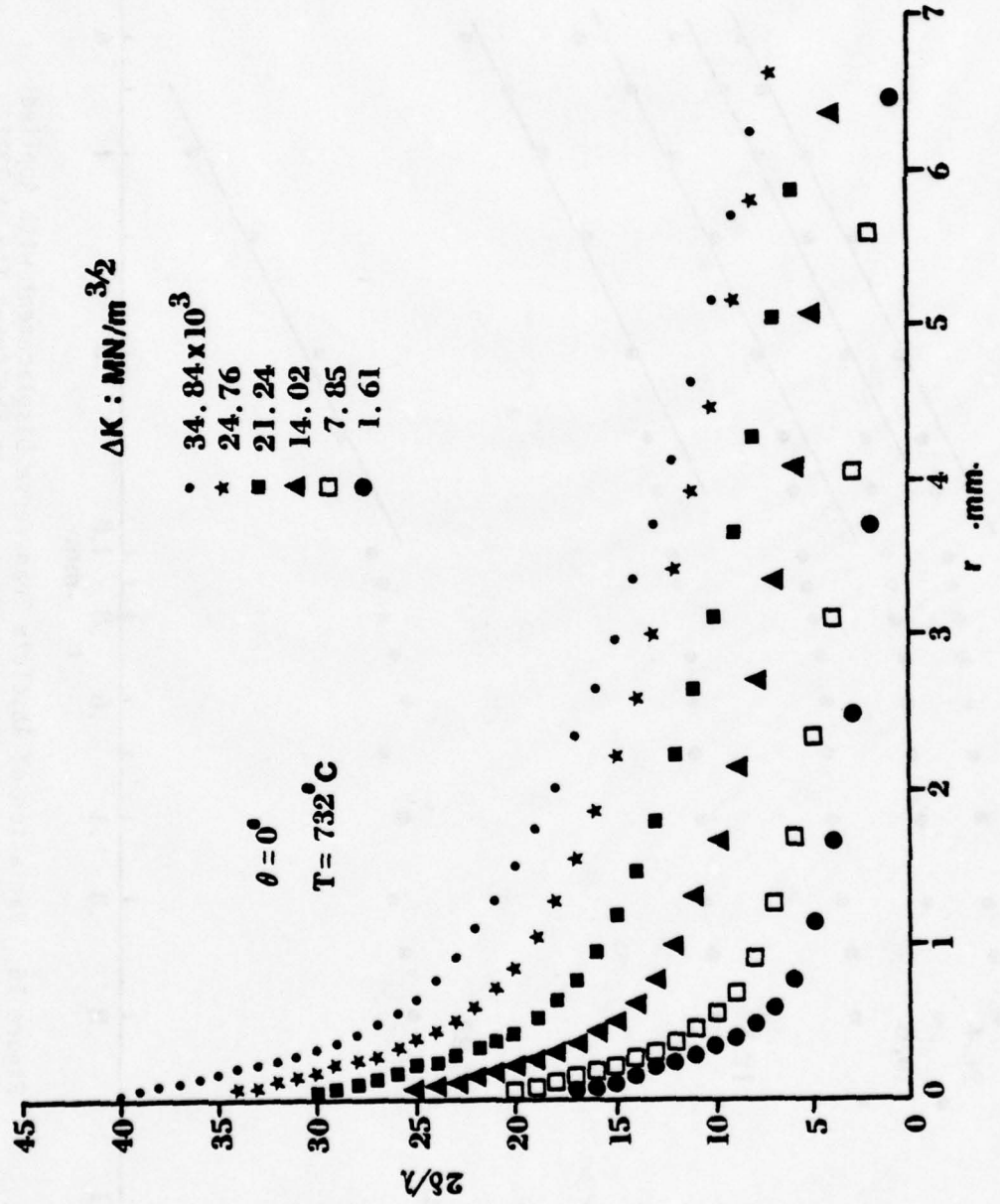

Figure 15. Variation of Transverse Displacement with Applied Stress Intensity and Distance from the Crack Tip at 732°C.

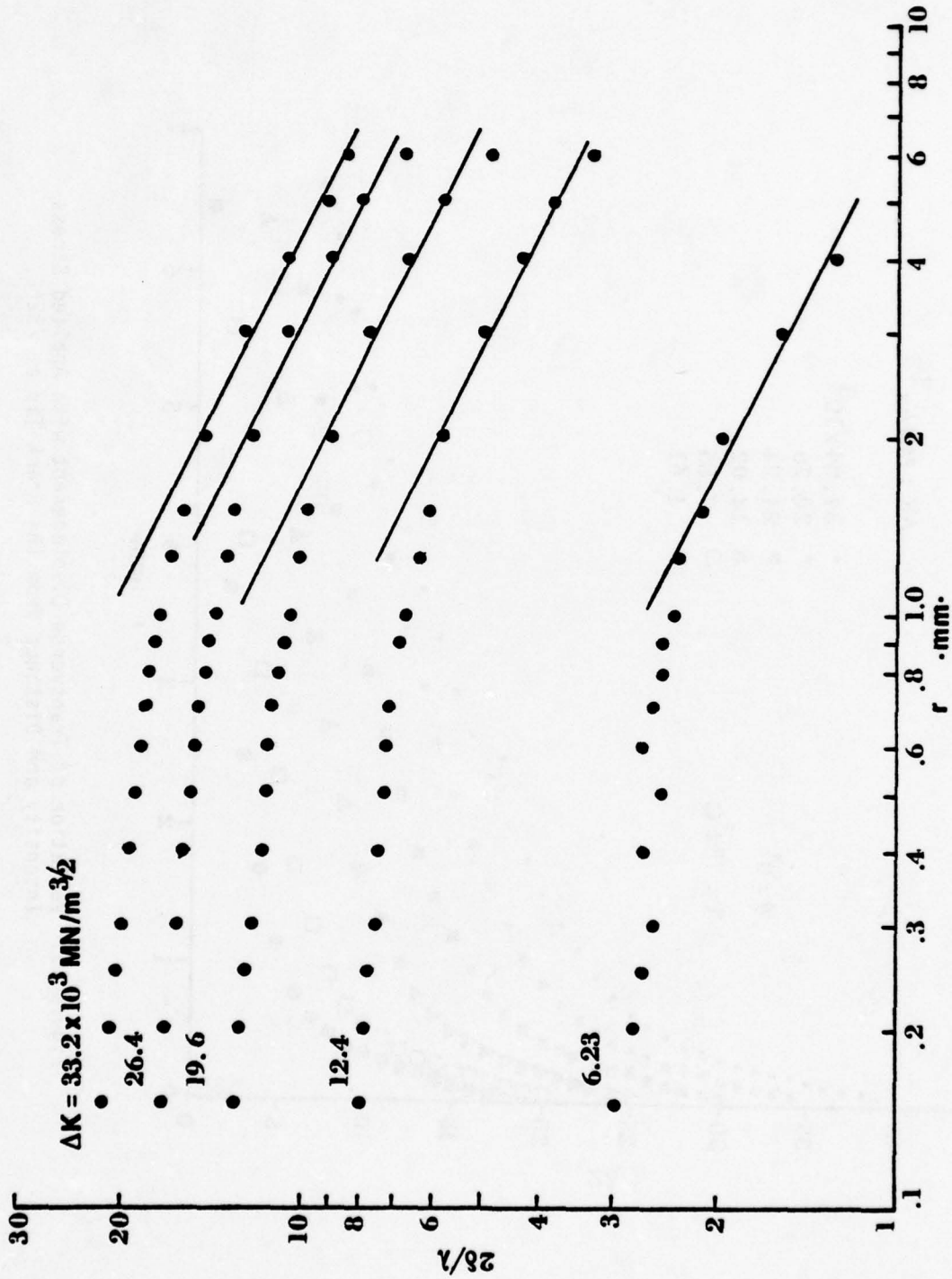

Figure 16. Variation of Absolute Transverse Displacement with Applied Stress Intensity and Distance from the Crack Tip at 732°C

Ke and Liu (Reference 30) have also found for a variety of specimen configurations that in a region near the crack tip the in-plane strain varies as $1/\sqrt{r}$. However, at greater distances from the crack tip the gradient was even steeper in agreement with the findings of this study.

2. REAL-TIME DISPLACEMENT MEASUREMENTS

a. Ambient Temperature

The analysis of the interference patterns as described previously is necessary to obtain information about the general behavior of the crack tip displacement field. However, the procedure is too time consuming to allow complete characterization of the displacement-load response at selected locations around the crack tip. To overcome this shortcoming a real-time analysis as described in Section IV was conducted. Two major features of the real-time displacement-load data emerged: (1) a nonlinear displacement-load behavior at low applied loads was observed and (2) near the crack tip the displacement-load response exhibited a hysteresis behavior.

Figure 17 is a typical plot of the displacement-load behavior at a point ahead of the crack tip for all crack lengths tested. At low loads a transition from nonlinear to linear behavior occurs. The load at this transition, P_{op}, can be interpreted as the load at which the crack faces are completely open. Crack closure, first observed by Elber (Reference 31) has been used successfully to explain the effect of stress ratio on fatigue crack propagation rate and has also provided an explanation for crack growth retardation resulting from an overload. Consequently, there is considerable interest in quantifying the magnitude of crack closure. When the data from all crack lengths and at several locations ahead of the crack is combined, it is found that the value of P_{op} varies with measurement location. It is highest at the crack tip and decreases as the distance from the crack tip increases.

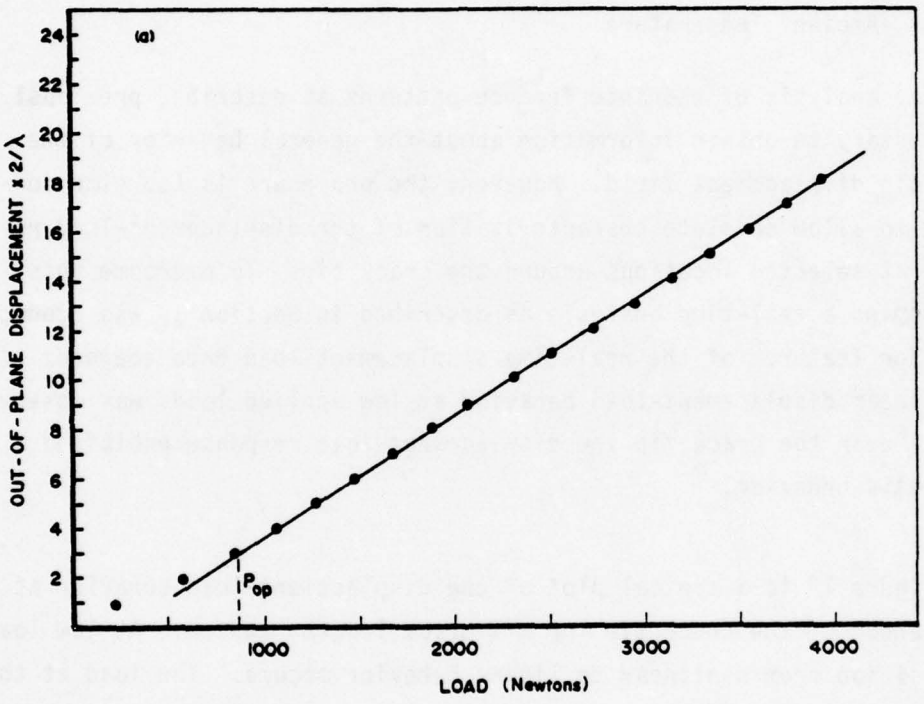

Figure 17. Typical Plot of Transverse-Displacement Load Behavior at Constant r Determined from Real-Time Analysis. Reference 32.

Simultaneous determinations of crack opening response were made on the specimen used in this study by the author's colleagues at the Air Force Materials Laboratory. P_{op} values were determined along the crack line behind the crack tip by D. E. Macha using an interferometric displacement gage technique (IDG) and at the crack mouth by D. M. Corbly using a clip-on displacement transducer. The data from all such measurements is shown in Figure 18 and is taken from Reference 32. Note, that away from the crack tip the value of P_{op}/P_{max} is independent of measurement location. However, near the crack tip a small change in measurement location can have a pronounced effect on the value of P_{op} determined. This has obvious significance to the determination of the magnitude of crack closure by displacement measurement techniques. Details of the measurement of P_{op} as discussed previously are given in References 32 and 33.

The existence of hysteresis behavior in the transverse displacement-load response near the crack tip is shown in Figure 19 for several locations ahead of the crack tip. Figure 19a gives the maximum displacement-load behavior. In all cases the location of maximum displacement was denoted by the origin of new fringes during loading and occurred at the crack tip. At all other locations the motion of fringes past the microhardness indentations (Figure 12) allowed the determination of the displacement-load response. The width of the hysteresis loop is maximum at the crack tip and decreases as the distance from the crack tip increases. If it is assumed that the hysteresis response results from reversed plasticity near the crack tip then the extent of hysteresis behavior should determine the extent of the reversed or cyclic plastic zone. Examination of Figure 19 indicates the disappearance of the hysteresis behavior at approximately $r = 0.45$ mm. An exact value is difficult to determine in a totally objective manner. However, this value appears to be a reasonable estimation from the data.

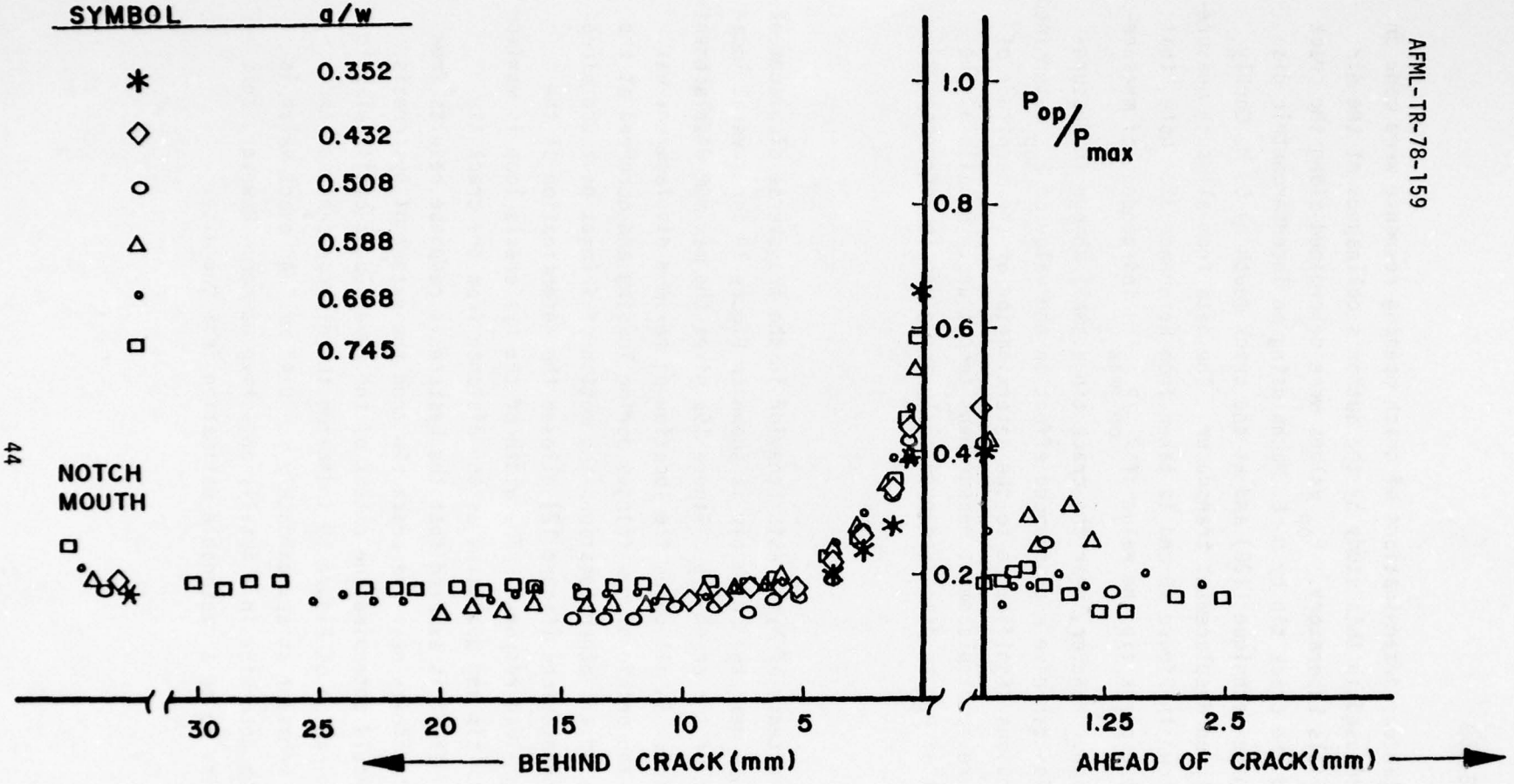

Figure 18. Composite Plot of the Variation of P_{op}/P_{max} with r for all Crack Lengths Tested. Reference 32.

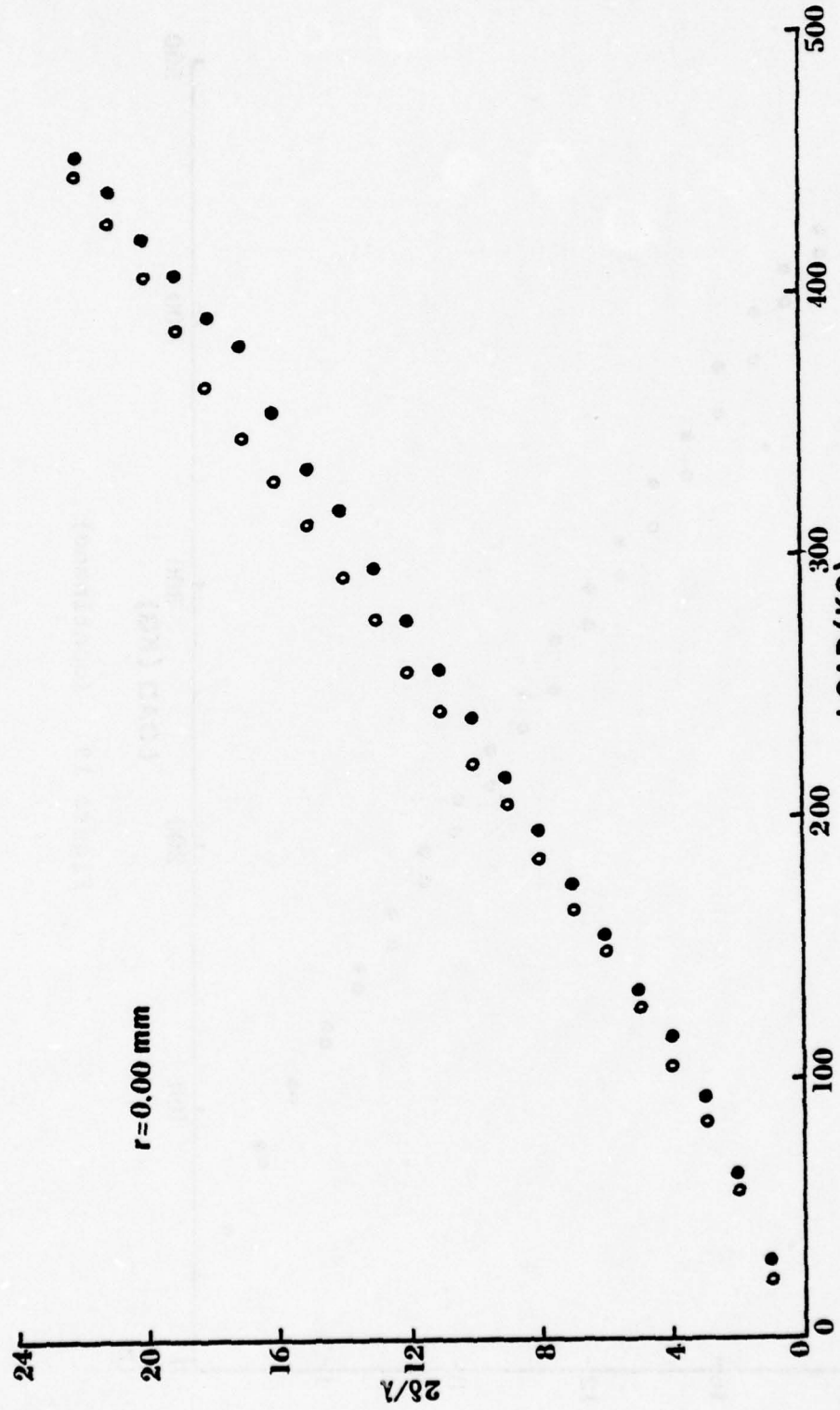

Figure 19. Transverse Displacement-Load Response as a Function of Distance from the Crack Tip. $\theta = 0°$.

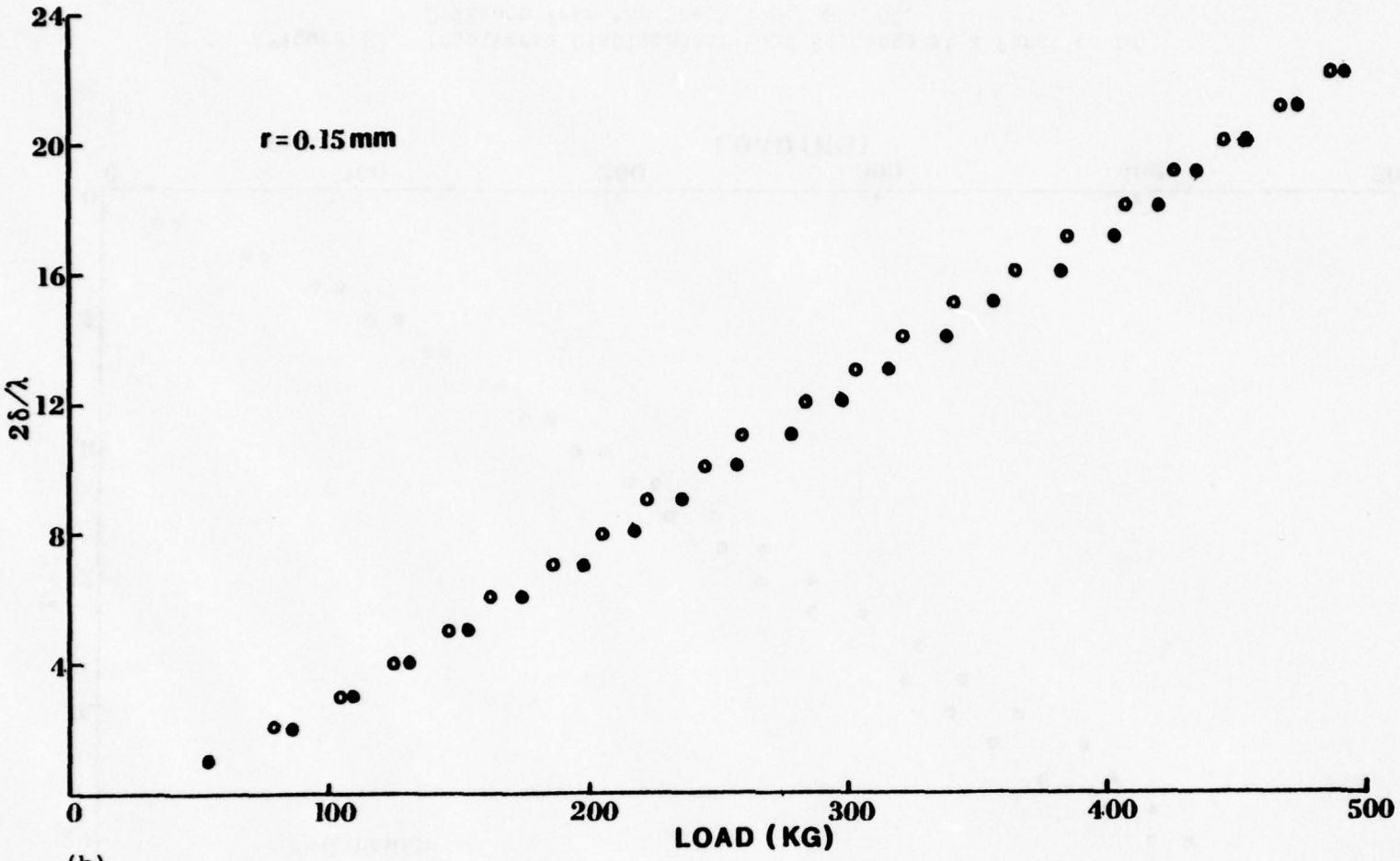

(b)

Figure 19. (continued)

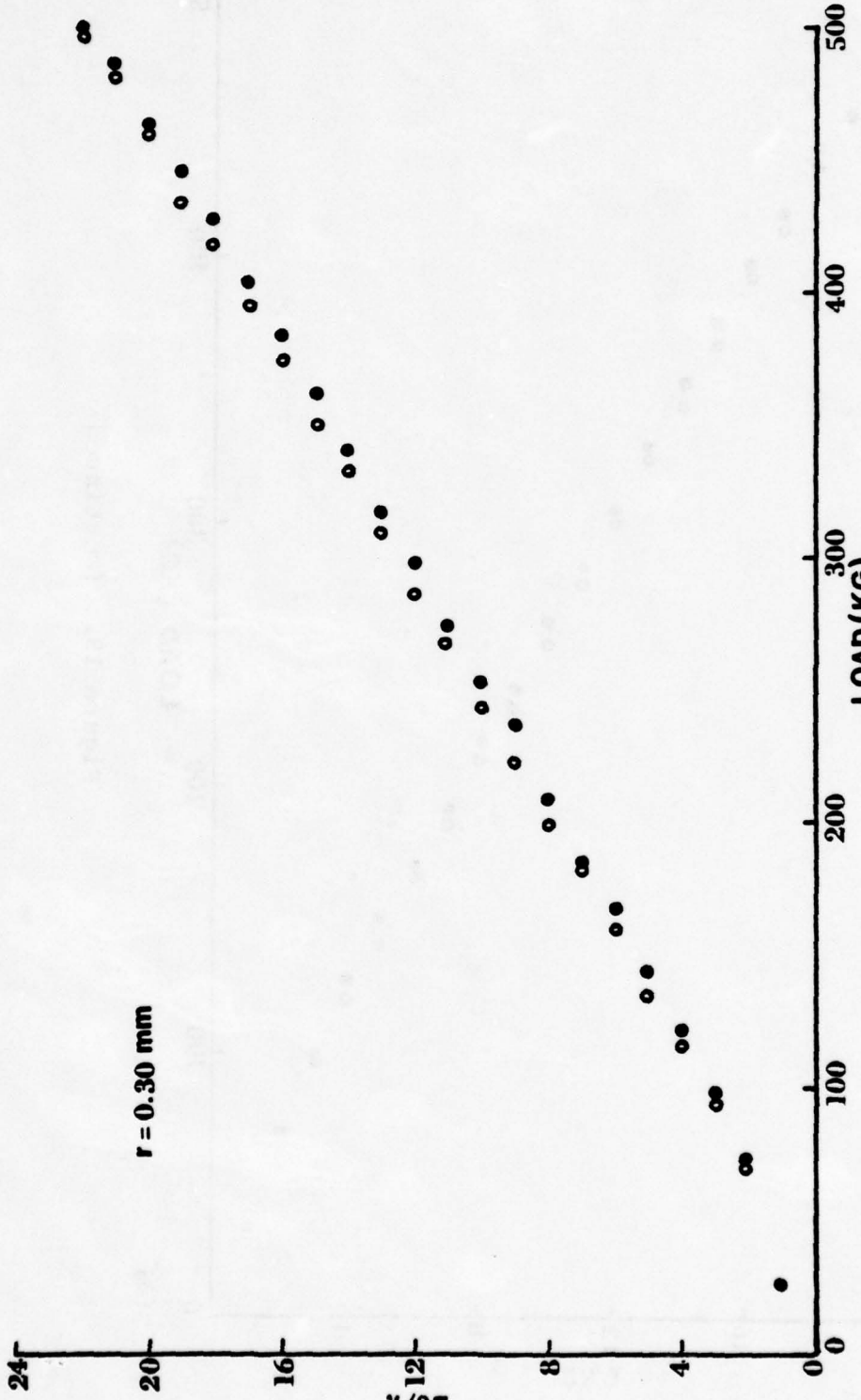

(c)

Figure 19. (continued)

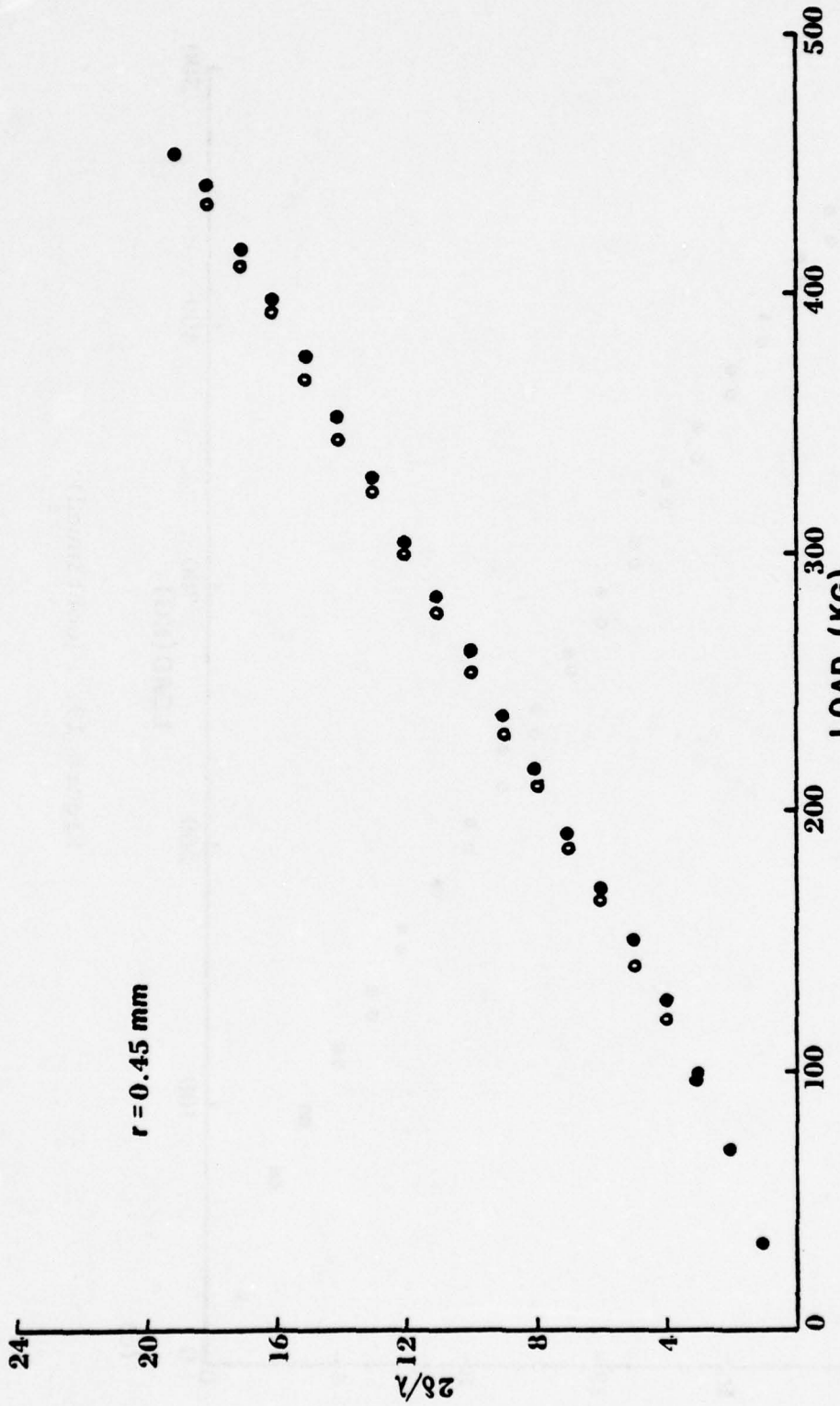

Figure 19. (continued)

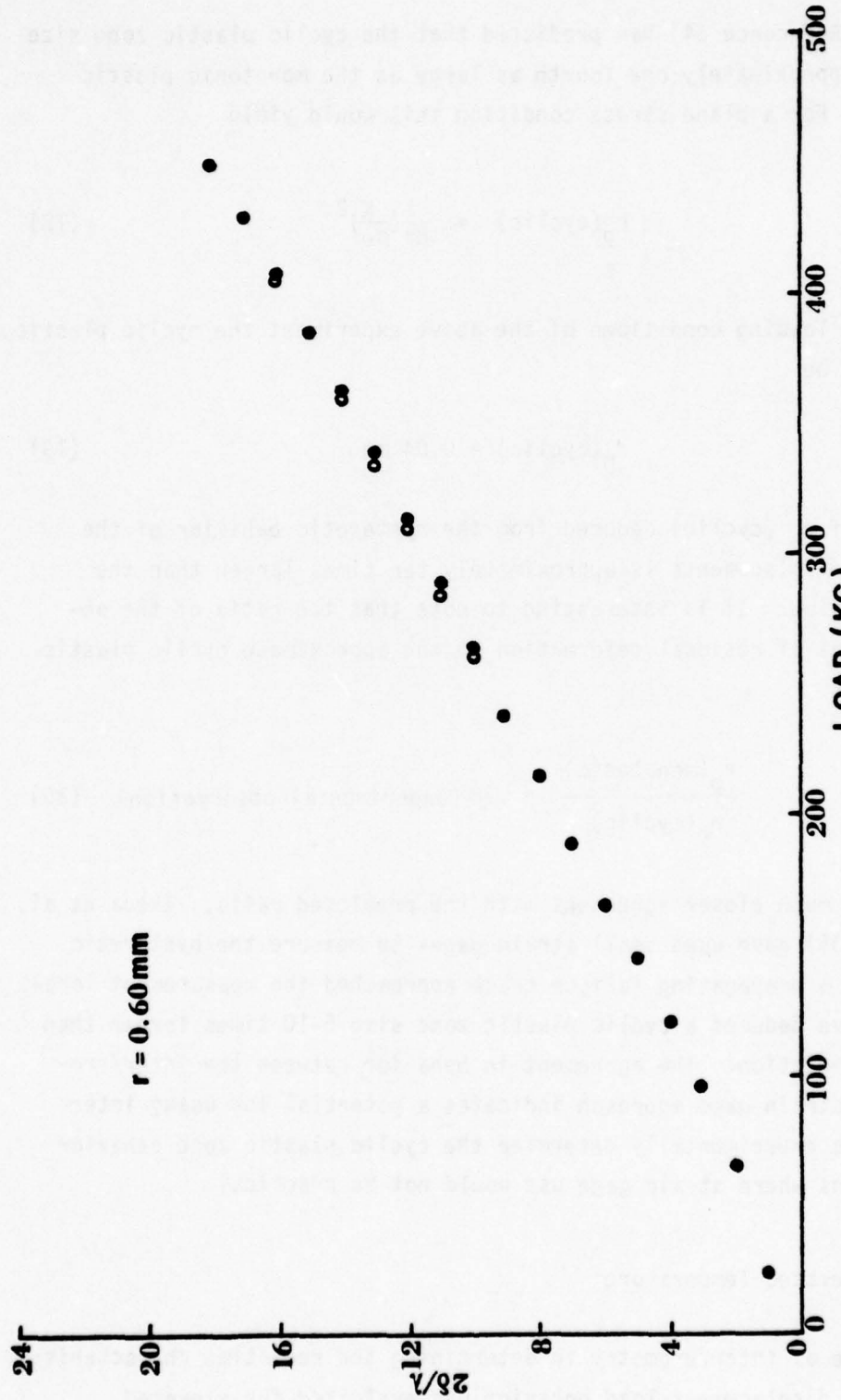

Figure 19. (continued)

Rice (Reference 34) has predicted that the cyclic plastic zone size should be approximately one fourth as large as the monotonic plastic zone size. For a plane stress condition this would yield

$$r_p(\text{cyclic}) \simeq \frac{1}{8\pi}\left(\frac{K}{\sigma_y}\right)^2 \tag{18}$$

and for the loading conditions of the above experiment the cyclic plastic zone should be

$$r_p(\text{cyclic}) = 0.04 \text{ mm} \tag{19}$$

The value of r_p (cyclic) deduced from the hysteretic behavior of the transverse displacements is approximately ten times larger than the predicted value. It is interesting to note that the ratio of the observed extent of residual deformation to the approximate cyclic plastic zone size is

$$\frac{r_p(\text{monotonic})}{r_p(\text{cyclic})} = .38 \text{ (experimental observation)} \tag{20}$$

which is in much closer agreement with the predicted ratio. Ikeda et al. (Reference 35) have used small strain gages to measure the hysteretic behavior as a propagating fatigue crack approached the measurement location and have deduced a cyclic plastic zone size 5-10 times larger than the Rice prediction. The agreement in behavior between the interferometric and strain gage approach indicates a potential for using interferometry to experimentally determine the cyclic plastic zone behavior in situations where strain gage use would not be practical.

b. Elevated Temperature

The use of interferometry in determining the real-time characteristics of the displacement-load behavior was evaluated for elevated

temperature testing. Data was obtained for the IN-100 specimen at temperatures of 538, 649, and 732°C. The results for the loading portion of the cycle are shown in Figure 20 for two values of r. Note that as the temperature increased the displacement at a given load also increased reflecting the change in Young's modulus. Although it was originally intended to monitor time dependent deformation in IN-100 at elevated temperatures under constant load, the stress and temperature conditions set for the study were apparently not severe enough to produce measurable time dependent deformation near the crack tip. Hold times as long as one hour produced no significant motion of the interference fringes. In addition, no detectable time dependent crack opening was observed using the IDG technique mentioned earlier. However, in a separate experiment it was possible using the optical interferometry technique to observe time dependent deformation near the crack tip in a titanium alloy stressed at ambient temperature! Thus, the optical interferometric determination of real-time displacements is possible given that creep deformation is occurring.

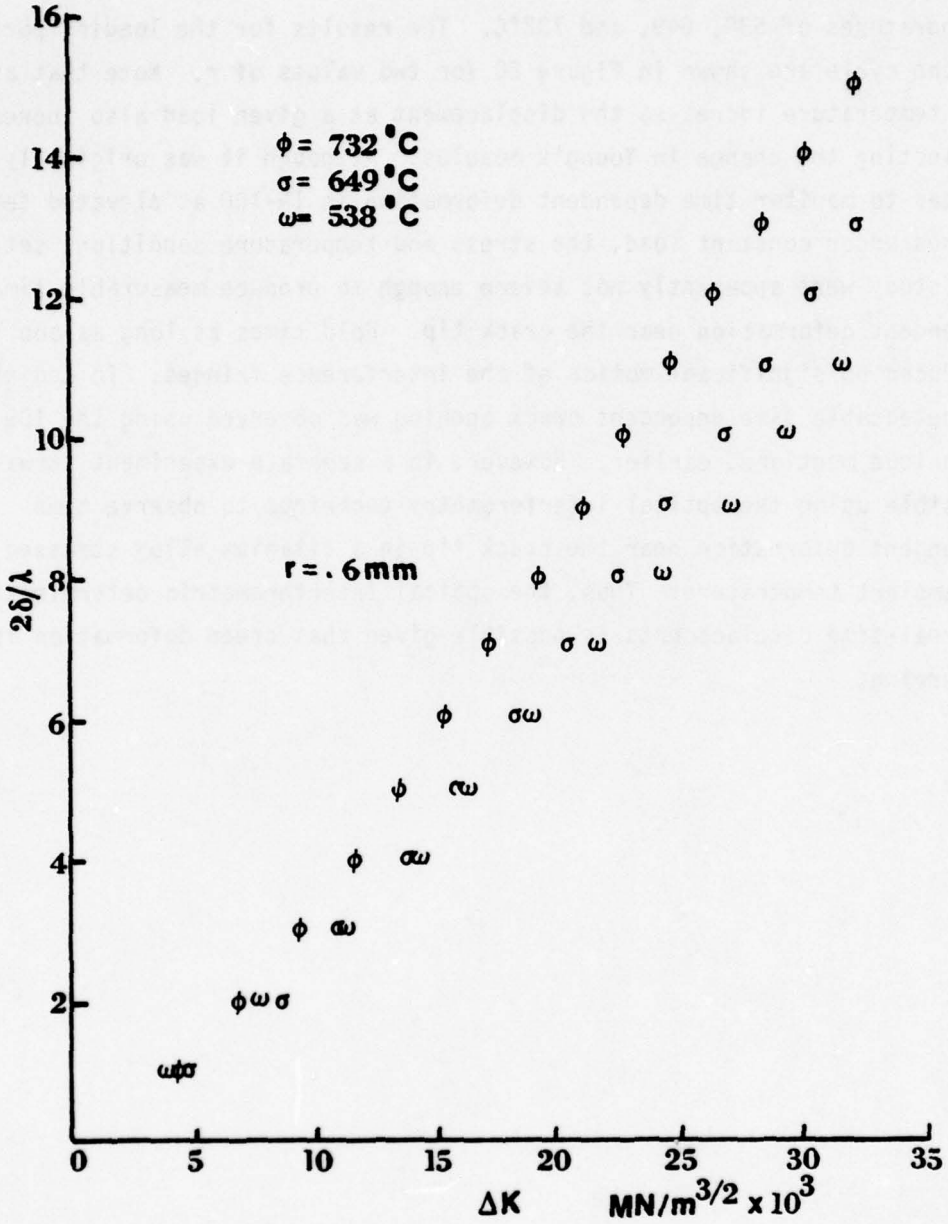

(a) r = 0.6 mm

Figure 20. Transverse Displacement Load Behavior at Two Locations Ahead of a Crack Tip at Three Temperatures. (a) r = 0.6 mm, (b) r = 2.1 mm.

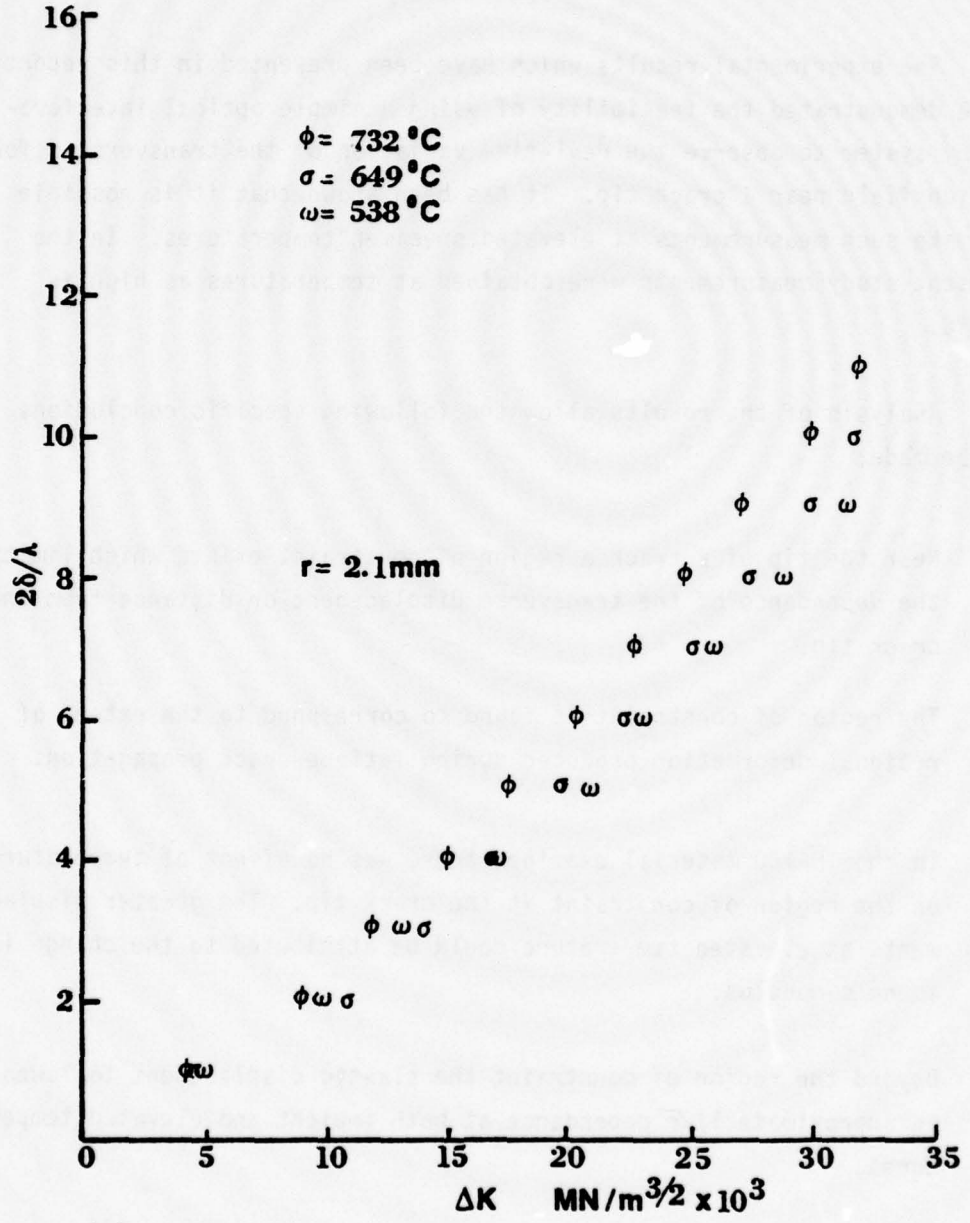

(b) r = 2.1 mm

Figure 20. (continued)

SECTION VI

CONCLUSIONS

The experimental results which have been presented in this report have demonstrated the feasibility of using a simple optical interferometry system to observe the real-time variation of the transverse deformation field near a crack tip. It has been shown that it is possible to make such measurements at elevated specimen temperatures. In the present study measurements were obtained at temperatures as high as 732°C.

Analysis of the results allow the following specific conclusions to be made:

1. Near the tip of a crack a region of constraint exists which limits the dependence of the transverse displacement on distance from the crack tip.

2. The region of constraint is found to correspond to the extent of residual deformation produced during fatigue crack propagation.

3. In the IN-100 material examined there was no effect of temperature on the region of constraint at the crack tip. The greater displacements at elevated temperature could be attributed to the change in Young's modulus.

4. Beyond the region of constraint the elastic displacement followed an approximate $1/\sqrt{r}$ dependence at both ambient and elevated temperatures.

5. The displacement variation with applied stress intensity at a point ahead of the crack tip indicated that for the 12.5 mm thick specimens tested only 3.5 - 3.8 mm near the surface could be considered as deforming in plane stress. This is considerably greater than the width of the shear lips formed and merits further study.

6. Real-time displacement-load results indicated that the crack opening load, P_{op}, was not a constant but depended on measurement location.

7. Preliminary results indicate that real-time transverse displacement measurements within the crack tip plastic zone can be used to delineate the cyclic plastic zone.

8. The cyclic plastic zone determined was an order of magnitude larger than the predicted zone size but the ratio of measured cyclic plastic zone to measured monotonic plastic zone was close to the theoretically predicted ratio.

APPENDIX A

INTERPRETATION OF DISPLACEMENT DATA FROM INTERFERROMETRIC MEASUREMENTS

One of the primary purposes of obtaining displacement data in the vicinity of the crack tip is to allow comparison with existing data and theoretical predictions. Although in principle it is possible to determine the first order fringe in an interference pattern this is often difficult to do experimentally. Usually a fringe order of one is assigned to the farthest fringe from the crack tip which is observable. The following simple argument illustrates that significant error can be introduced if this procedure is employed in the determination of the dependence of displacement on distance from the crack tip.

Consider the displacement in the crack tip region to obey the relation

$$\delta = C\sigma r^n \tag{A.1}$$

where C depends on crack length, σ is the nominal applied stress, r is the distance from the crack tip and n is a real number. The change in the displacement field on increasing the applied stress from σ_1 to σ_2 will be given by

$$d\delta = Cd\sigma r^n \tag{A.2}$$

Thus for a given $d\sigma$ the variation of $d\delta$ with r depends on n where $d\delta = \delta_{\sigma 2} - \delta_{\sigma 1}$ and $d\sigma = \sigma_2 - \sigma_1$. σ_1 is taken different from zero simply for the sake of generality. It is a simple matter to determine the exponent, n, in Equation A.2 by plotting the experimentally determined displacement data on log-log coordinates and graphically determining the slope of the resulting curve. The value of the slope is numerically equivalent to n and is given by

$$n = \frac{\log(d\delta(r_2) - \log(d\delta(r_1))}{\log r_2 - \log r_1} \tag{A.3}$$

where r_2 and r_1 are, respectively, the maximum and minimum distances from the crack tip in the field of observation.

Now assume that a constant displacement, Δ, is added to the displacement field produced by σ_2. This is equivalent to "assigning" an arbitrary order to the fringes. The displacement-distance relation for σ_2 is now given by

$$\delta = C\sigma_2 r^n + \Delta \tag{A.4}$$

and the exponent, n', is given for this case as

$$n' = \frac{\log(d\delta(r_2) - \Delta) - \log(d\delta(r_1) - \Delta)}{\log r_2 - \log r_2} \tag{A.5}$$

That n' can significantly differ from n is illustrated in the following simplistic example. Consider a perfectly elastic material containing a crack. Assuming plane stress the in-plane stresses are

$$\sigma_{xx} = \frac{K_I}{\sqrt{2\pi r}} \cos\frac{\theta}{2} \left[1 - \sin\frac{\theta}{2} \sin\frac{3\theta}{2}\right] \tag{A.6}$$

$$\sigma_{yy} = \frac{K_I}{\sqrt{2\pi r}} \cos\frac{\theta}{2} \left[1 - \sin\frac{\theta}{2} \sin\frac{3\theta}{2}\right]$$

and recalling that the transverse strain field can be expressed as

$$\varepsilon_{zz} = \frac{-\nu}{E} (\sigma_{xx} + \sigma_{yy}) \tag{A.7}$$

it is possible to determine the transverse displacement field. For the example chosen let K = 33 MPa $\sqrt{m}$, ν = 0.3, and E = 2.06 x 10^5 MPa. The limits to the field of observation along the plane of the crack (θ = 0) can be reasonably approximated as r_1 = 0.254 mm (.01 in) and r_2 = 5.08 mm (.2 in). From Equation A.6 the displacement at r_1 and r_2 is calculated by assuming the specimen thickness B = 7.62 mm (.3 in).

r (mm)	σ_{xx} (MPa)	σ_{yy} (MPa)	ε_{zz}	$\delta = \frac{\varepsilon_{zz}}{2} B$
0.254	827	827	2.4×10^{-3}	9.14×10^{-6} m
5.08	185	185	5.36×10^{-4}	2.04×10^{-6} m

The variation of δ with r for this case is shown as the solid line in Figure A.1. If the nearest constructive fringe to r = 0.20 in is given the order of one then the presumed displacement at that point is $\lambda/2$ or $.2946 \times 10^{-6}$ m (for sodium vapor illumination). This presumed displacement field is shown in Figure A.1 as the dashed curve. The difference between the actual and presumed displacement field is approximately 1.75×10^{-6} m. Calculation of n' from the presumed displacement field yields from Equation A.5.

$$n' = -1.40 \tag{A.8}$$

which is totally different from the value of n = -0.5 imposed by this example. Note that the actual fringe order at r = 5.08 mm is approximately seven.

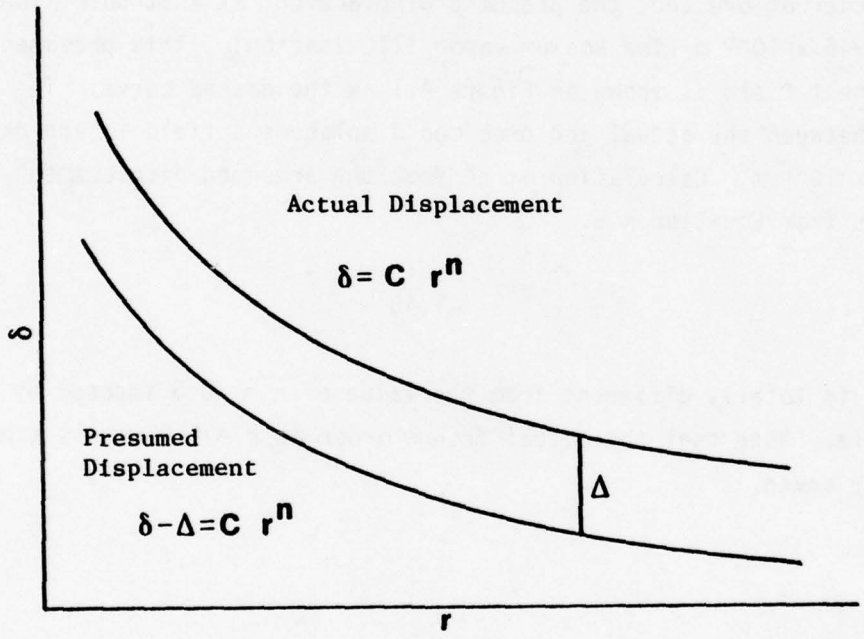

Figure A.1 Illustration of the Change in the Measured Displacement Field by Arbitrarily Determining Fringe Order

APPENDIX B
ANALYSIS OF INTERFEROGRAMS BY THE MOIRE´ METHOD

As stated in Appendix A, proper analysis of optical interference patterns to obtain absolute out-of-plane displacement data requires that the relative fringe order be known at each applied load investigated. This section discusses further complications in the interpretations of interference patterns and demonstrates a novel approach to circumventing these problems.

1. FACTORS AFFECTING THE APPARENT DISPLACEMENT FIELD

Consider the region near a crack tip to be planar and perpendicular to the transverse direction at zero applied stress. Consider also that a perfectly flat quartz plate rests on the specimen surface in the crack tip region. Under stress the total separation of quartz plate and specimen surface results from transverse specimen contraction and can be expressed as

$$h(x,y) = g_1(x,y) = n\frac{\lambda}{2} \tag{B.1}$$

where $h(x,y)$ is the total separation, $g_1(x,y)$ represents the specimen contraction in the transverse direction and x,y are coordinates in the plane of the specimen surface.

Experimentally, the above conditions will seldom be perfectly satisfied and the total displacement between optical flat and specimen surface can be described as the sum of three distinct displacement fields as

$$h(x,y) = g_1(x,y) + g_2(x,y) + g_3(x,y) \tag{B.2}$$

where, as shown in Figure B.1, $g_2(x,y)$ represents the deviation of the specimen surface from a planar surface and $g_3(x,y)$ represents a tilt of the optical flat from the presumed planar surface. $g_2(x,y)$ and $g_3(x,y)$ can combine to make the determination of the true displacement

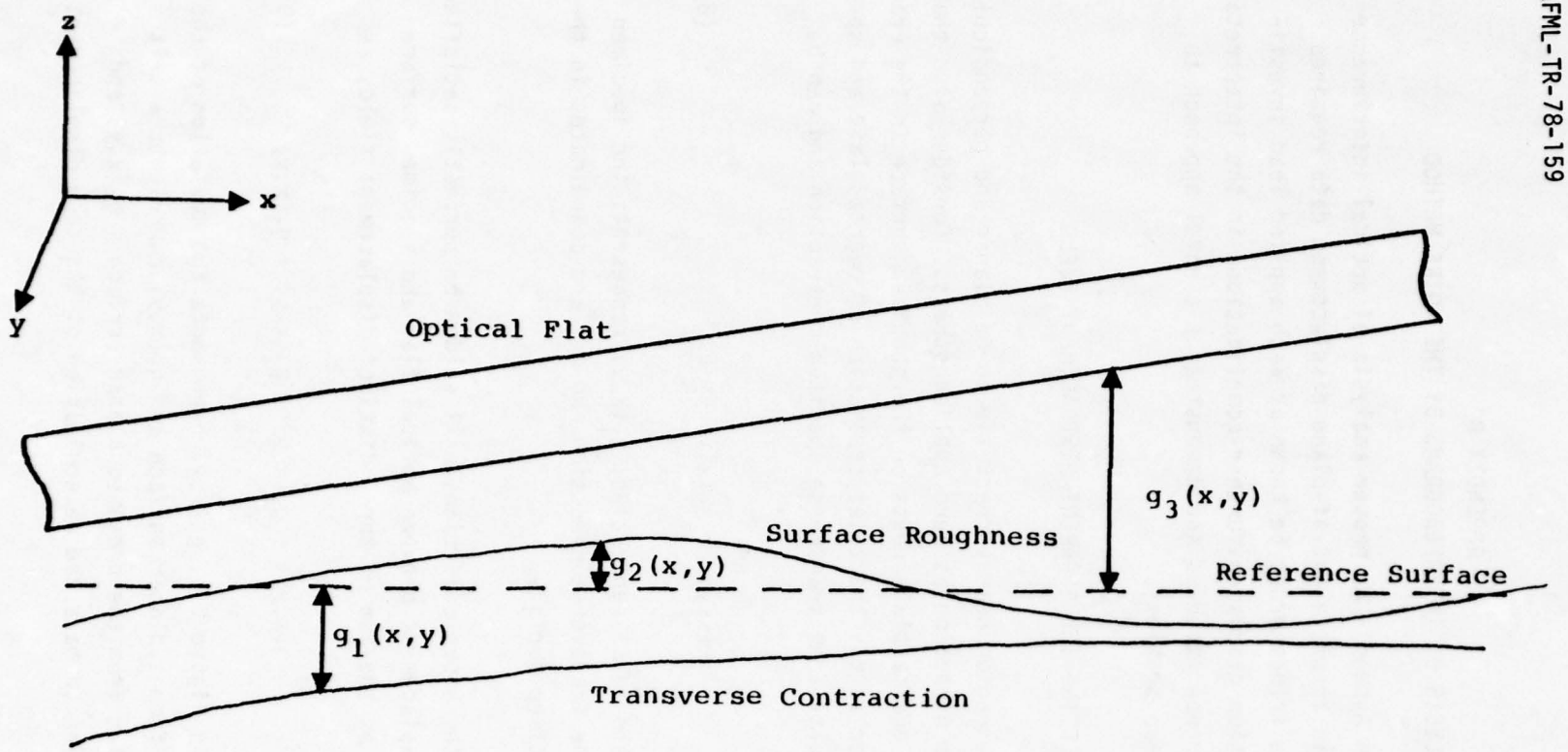

Figure B.1 Illustration of the Various Experimental Factors Which Can Influence the Measurement of Displacement Changes Using Interferometry.

field, $g_1(x,y)$, very difficult. Only when $g_2(x,y)$ and $g_3(x,y)$ are small compared to $g_1(x,y)$ can the true displacement field be determined directly from the observed fringe pattern. For the surface quality and the magnitude of displacements studied in this report the direct determinations of displacements are possible. If, however, displacement changes on the order of $\lambda/2$ over the area of observation are to be measured, serious error can result from the digitization and subsequent subtraction of presumed displacement fields when the perturbations in the fringe patterns resulting from $g_2(x,y)$ and $g_3(x,y)$ are not considered. This results in part from the fact that for an interference pattern with a low fringe density the selection of an interpolation function to allow subtraction of two interference patterns will strongly influence the resultant displacement field.

2. ANALOGY BETWEEN MOIRÉ ANALYSIS AND INTERFERENCE PATTERNS

The difficulties described previously can be overcome by imposing an artificially high fringe density (increasing the contribution of $g_3(x,y)$) and treating the resultant fringe patterns as moiré gratings. Subsequent superposition of two such "gratings" produced at different applied stresses will be shown to yield the net displacement change between the two stresses.

The moiré method of strain analysis involves placing a dense grid of lines on the specimen surface such that the line density is known. When the specimen undergoes elongation normal to the line in the grid a new grid spacing is produced. Light transmitted through or reflected from the deformed grating and an undeformed master grating produces a series of interference fringes. The order of the fringes can be related to the in-plane displacement, u, by (Reference 36).

$$u = \frac{N}{P} \qquad (B.3)$$

where N is the fringe order and P is the pitch (lines/cm) of the master grating. The sensitivity of the technique depends on the spacing of the lines in the master grating. The distance between the moiré fringes is

$$d = \frac{P_1 P}{P_1 - P} \tag{B.4}$$

where P_1 is the pitch of the deformed grating.

An optical interferometry analogy to moiré analysis can be constructed as follows. An evenly spaced fringe pattern is produced by inclining an optical flat relative to a reflecting surface through an angle, α. The opening along the planar air wedge so produced is (Figure B.2)

$$\Delta = x \tan \alpha \tag{B.5}$$

and the condition for constructive fringe formation is

$$\frac{n\lambda}{2} = x \tan \alpha \tag{B.6}$$

The spacing between two adjacent fringes is

$$dx = x_n - x_{n-1} = \left(\frac{n\lambda}{2} - (n-1)\frac{\lambda}{2}\right)\cot \alpha \tag{B.7}$$

and, analogous to the moiré method, the pitch is given by

$$P_\alpha = dx = \frac{\lambda}{2} \cot \alpha \tag{B.8}$$

Changing the inclination of the optical flat by the small angle, δ, causes the new fringe spacing to become

$$P_{\alpha+\delta} = dx' = \frac{\lambda}{2} \cot (\alpha+\delta) \tag{B.9}$$

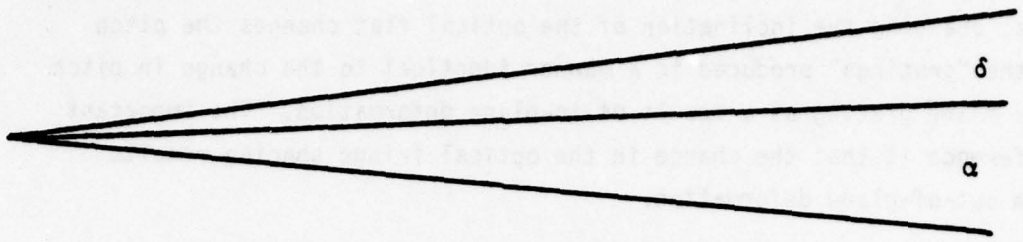

Figure B.2 Inclinations of an Optical Flat to Produce Changes in an Interference Pattern Which Are Analogous to the Deformation of a Moiré Grating

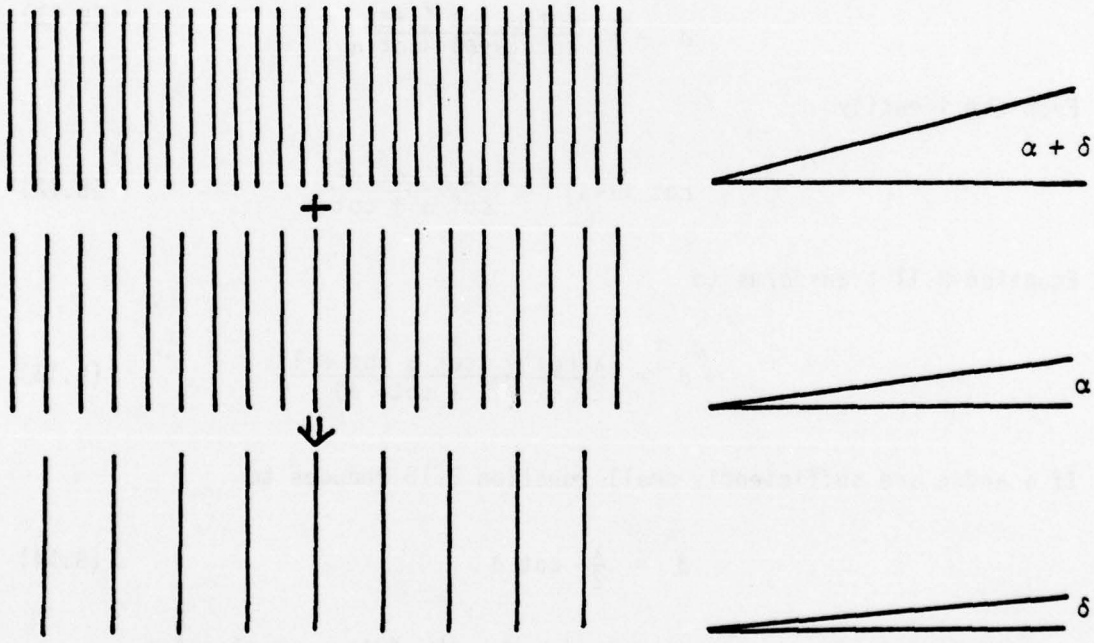

Figure B.3 Schematic of Optical Filtering Technique for Conditions Shown in Figure B.2.

Thus, changing the inclination of the optical flat changes the pitch of the "gratings" produced in a manner identical to the change in pitch of a moiré grating as a result of in-plane deformation. The important difference is that the change in the optical fringe spacing results from out-of-plane deformation.

Overlaying the fringe patterns produced at the two optical flat inclinations should produce a moiré pattern with fringe spacing

$$d = \frac{P_\alpha P_{\alpha+\delta}}{P_{\alpha+\delta} - P_\alpha} \tag{B.10}$$

Substituting Equations B.8 and B.9 into Equation B.10 yields

$$d = \frac{\lambda}{2} \frac{\cot \alpha \cot (\alpha+\delta)}{\cot (\alpha+\delta) - \cot \alpha} \tag{B.11}$$

From the identity

$$\cot (\alpha+\delta) = \frac{\cot \alpha \cot \delta - 1}{\cot \alpha + \cot \delta} \tag{B.12}$$

Equation B.11 transforms to

$$d = \frac{\lambda}{2} \frac{\cot \alpha (\cot \alpha \cot \delta - 1)}{-(1 + \cot^2 \delta)} \tag{B.13}$$

If α and δ are sufficiently small Equation B.13 reduces to

$$d = \frac{\lambda}{2} \cot \delta \tag{B.14}$$

Note, that this is simply the relation for the fringe spacing for an optical flat inclination of angle δ. This implies that the interference produced by the superposition of interferometrically constructed gratings will act as an optical filter to yield a measure of the net change in displacement. This is illustrated in Figure B.3 for the case discussed previously and in Figure B.4 for the common example of a groove in a flat surface.

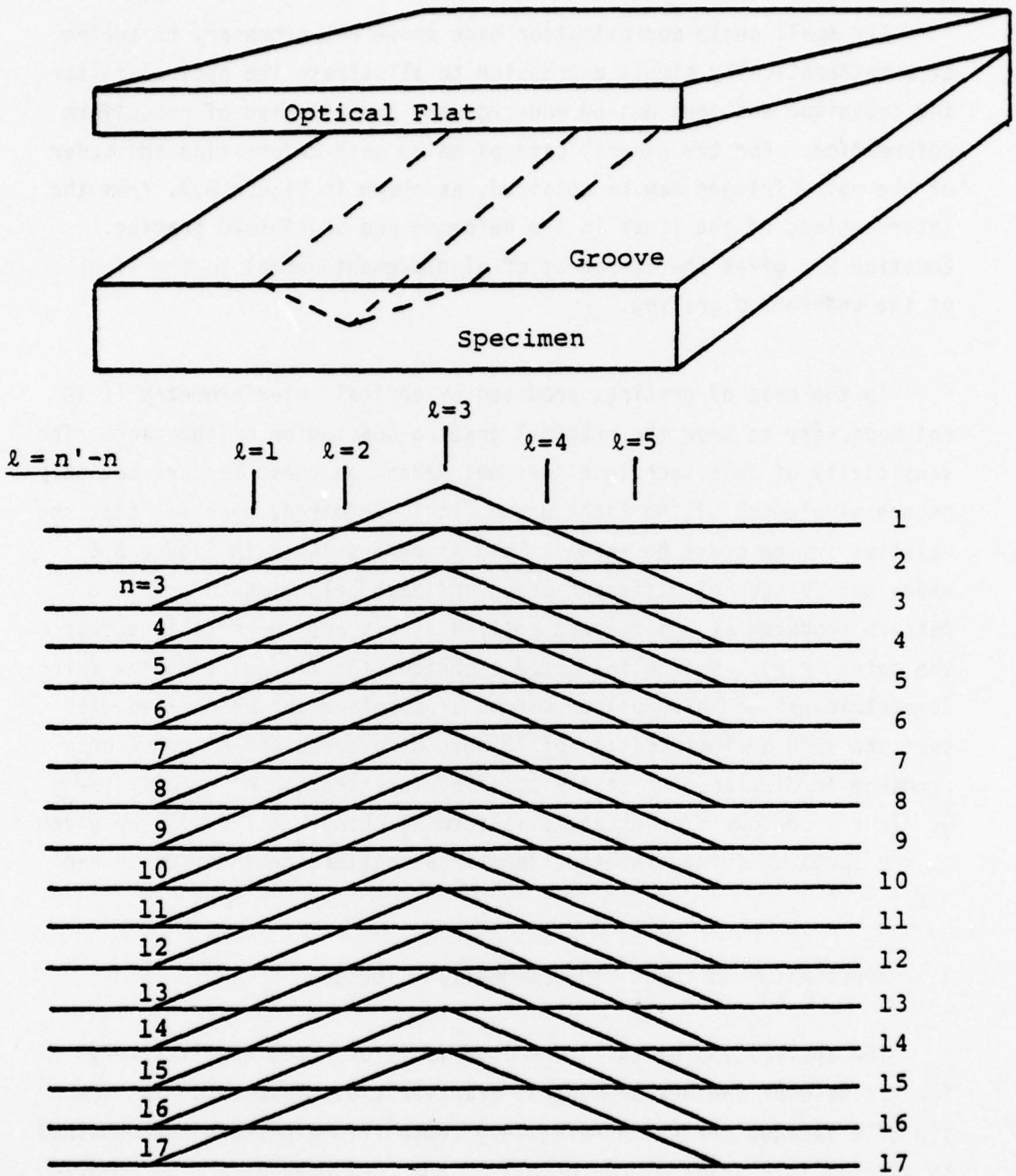

Figure B.4 Illustration of Optical Filtering Technique Indetermination of Displacements Induced in an Originally Flat Plate. Note, That the Moiré Pattern Produced Is Identical to the Interferometric Pattern Which Would Be Produced if the Optical Flat Was Placed in Registry with the Specimen Surface.

The small angle approximation made above was necessary to arrive at a mathematically simple expression to illustrate the optical filtering technique and need not be made for the general case of nonuniform deformation. For the general case of moiré grid deformation the order of the moiré fringes can be obtained, as shown in Figure B.5, from the intersections of the lines in the deformed and undeformed grating. Equation B.3 gives the component of displacement normal to the lines of the undeformed grating.

In the case of gratings produced by optical interferometry it is not necessary to know the original grating spacing or orientation. The sensitivity of this technique does not depend on these factors but only on the wavelength of the light used. It is required, however, that the relative fringe order be known. This is demonstrated in Figure B.6 where two fringes of different order and each belonging to a fringe pattern produced at a different applied stress are shown to intersect at the point (r,θ). Unlike the moiré technique the fringes from the interferometric pattern have unique values of displacement associated with them and such an intersection of fringes of order n and n' represents a change in displacement at the point of intersection of exactly $(n-n')\frac{\lambda}{2}$. Thus a contour of constant displacement change, $\ell\lambda/2$, will be given by the locus of fringe intersections whose difference in order is $n-n' = \ell$.

3. APPLICATION TO CRACK TIP DEFORMATION STUDIES

The application of this technique is illustrated qualitatively for the case of the measurement of transverse displacements near the tip of a fatigue crack. A relatively dense fringe pattern was obtained by placing thin shims at two points on the perimeter of a 2.54 cm diameter quartz optical flat. The optical flat contacted the specimen surface at a third point producing a small inclination with respect to the specimen surface. A modified compact specimen of IN-100 was used. Specimen size, preparation, and crack growth parameters are the

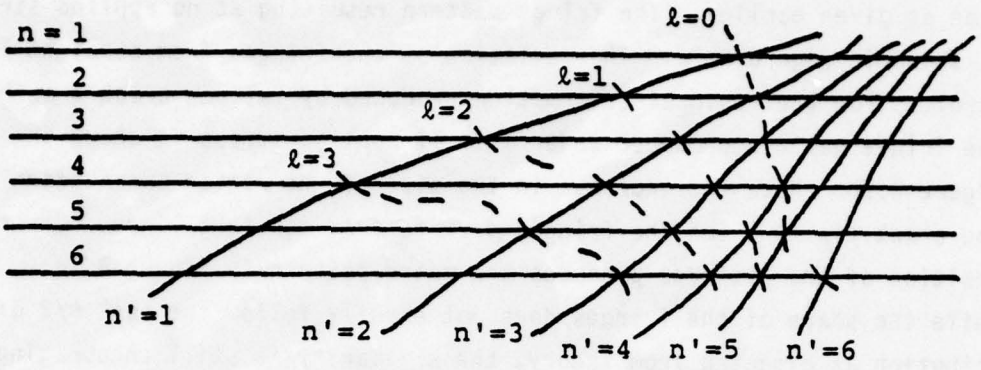

Figure B.5 Schematic Illustration of Nonuniform Deformation of a Moiré Grating.

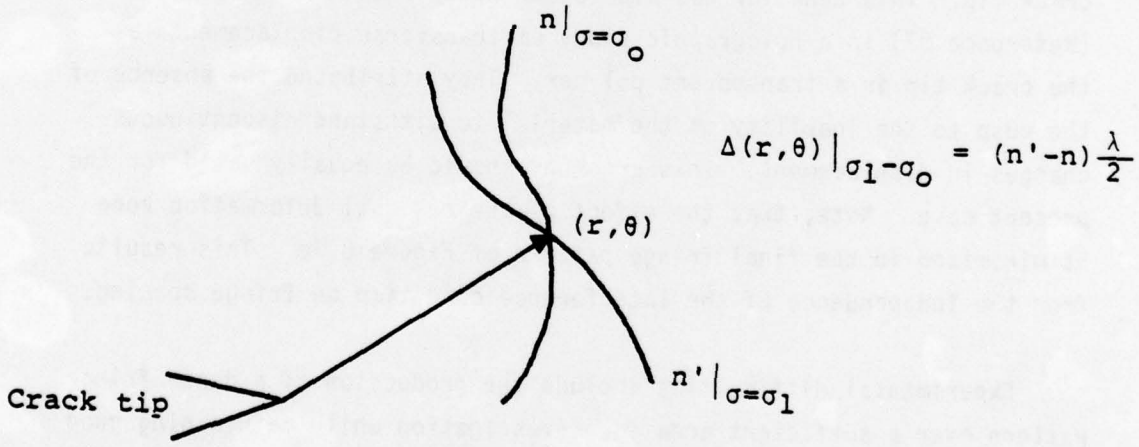

Figure B.6 Interference Analogy to Nonuniform Deformation of a Moiré Grating.

same as given earlier. The fringe pattern resulting at no applied stress is shown in Figure B.7a. The deviation of the fringes from straight lines results from the residual deformation produced by fatigue crack growth. The fringe pattern produced under a small applied stress is shown in Figure B.7b. Note the increase in the size of the region surrounding the crack tip in which the fringes deviate from straight lines. Superposition of the patterns produces the moiré pattern in Figure B.7c. While the shape of the fringes does not exactly follow the $\cos^2 \theta/2$ distribution as expected from theory, the similarity is still encouraging. By tracking far field fringes during loading the order of the moiré fringe nearest the crack tip was determined to be n= 7 which gives a displacement near the crack tip of 2.06 μm for the small stress applied.

Linear elastic fracture mechanics theory predicts the occurrence of a cusp in the strain field at the crack tip for $\theta = 180°$. In the example shown the cusp is absent and the fringes intersect behind the crack tip. This behavior was also observed by Dudderar and O'Regan (Reference 37) in a holographic study of transverse displacements at the crack tip in a transparent polymer. They attributed the absence of the cusp to the inability of the material to withstand discontinuous changes in displacement. This argument should be equally valid for the present case. Note, that the effect of the residual deformation zone is minimized in the final fringe pattern of Figure B.7c. This results from the independence of the interference condition on fringe spacing.

Experimental difficulties include the production of a dense fringe pattern over a sufficient area for investigation while maintaining good fringe contrast and the avoidance of rotation of the optical flat during loading. However, with proper caution these difficulties can be overcome. The technique should be well suited to the measurement of very small displacements, such as in the vicinity of holes and notches, where perfect surface flatness cannot be attained. The technique is simpler than the use of standard moiré techniques for the measurement of isopachics and considerably more sensitive.

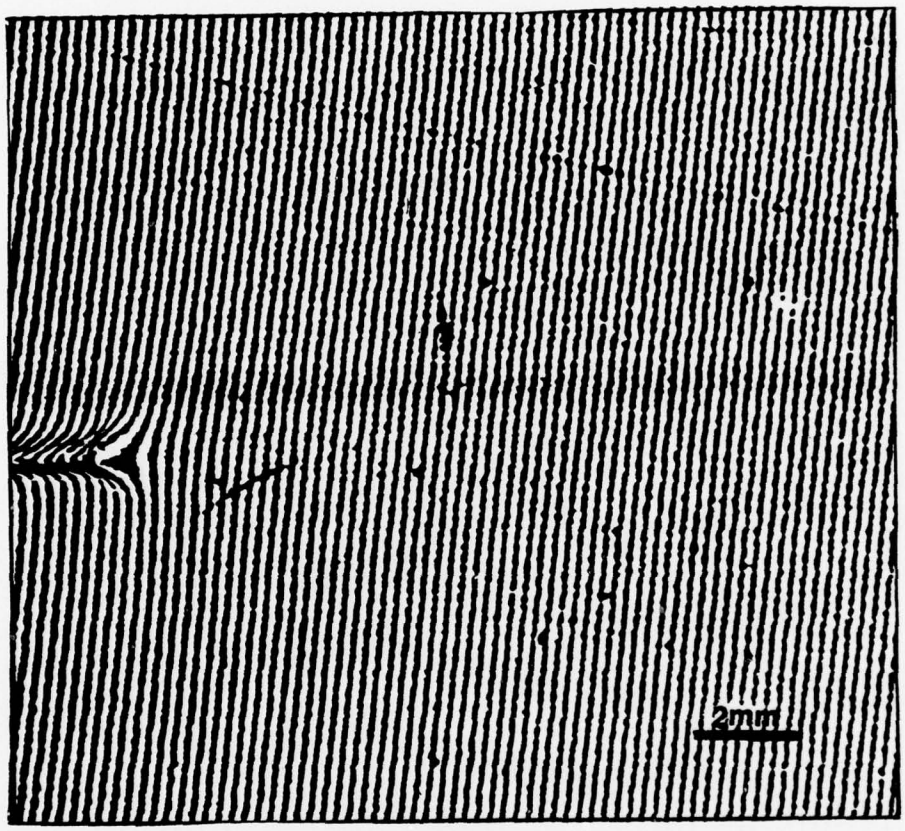

Figure B.7a Interferometrically Produced Grating for Fatigue Crack Under No Load Conditions. Crack Tip Is Discontinuity in Pattern at Left.

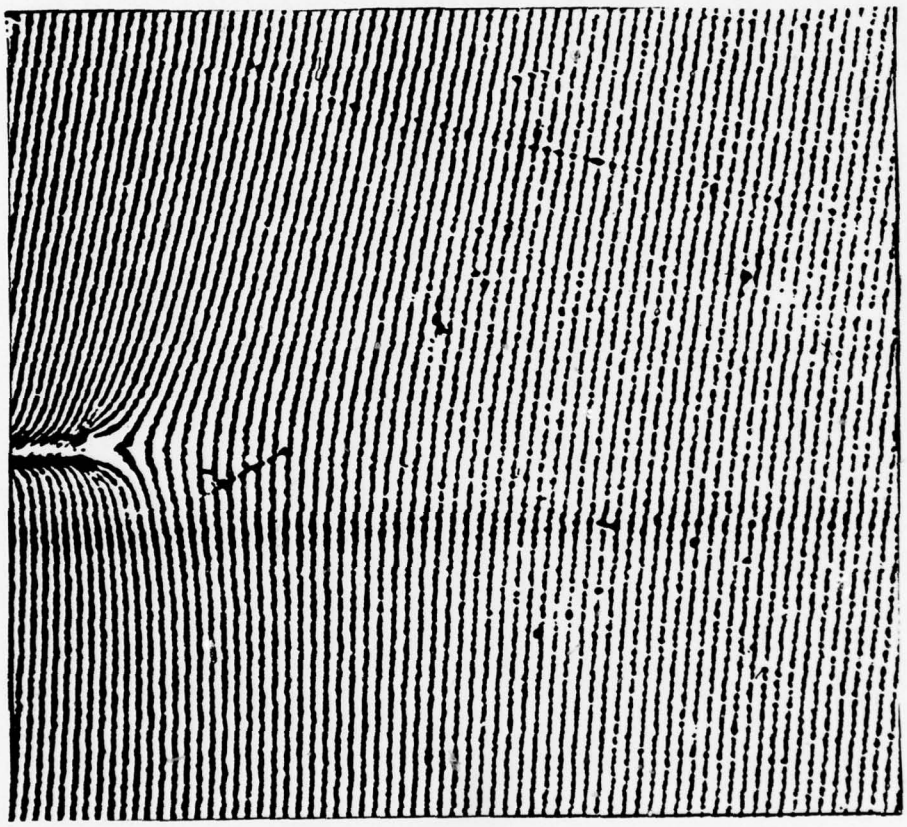

Figure B.7b Deformation of Interferometrically Produced Grating for Fatigue Crack Under Small Applied Load.

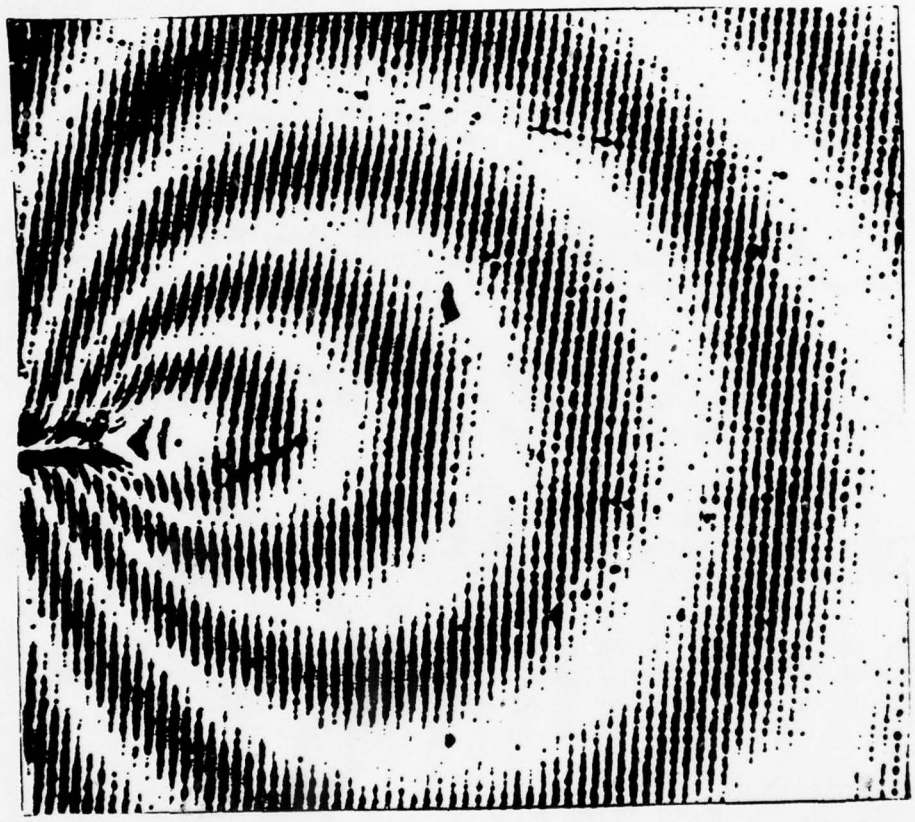

Figure B.7c Moiré Pattern of Isopachics Resulting from the Superpositions of the Gratings Shown in Figures B.7a and b. The Change in Specimen Half Thickness Is 0.2946 μm Per Fringe.

REFERENCES

1. M. J. Siverns and A. T. Price, "Crack Growth Under Creep Conditions," Nature, 228 (1970), 760-761.

2. H. G. Popp and A. Coles, Proc. U. S. Air Force Conf. on Fatigue and Fracture, AFFDL-TR-70-144, 1970, p. 71.

3. S. Floreen, "The Fracture of Wrought Nickel-Base Superalloy by a Fracture Mechanics Approach," Met. Trans., 6A (1975), 1744-1749.

4. G. J. Neate and M. J. Siverns, "The Applications of Fracture Mechanics to Creep Crack Growth," Int. Conf. on Creep and Fatigue in Elevated Temperature Applications, Philadelphia, 1973, and Sheffield, 1974.

5. J. G. Kaufman, K. O. Bogardus, D. A. Mauney, and R. C. Malcolm, "Creep Cracking in 2219-T851 Plate at Elevated Temperatures," ASTM STP590, Philadelphia, 1976, 149-168.

6. L. A. James, "Some Preliminary Observations on the Extension of Cracks Under Static Loading at Elevated Temperatures," Int. Journal Fracture Mech., 8 (1972), 347-349.

7. H. Kashiwaga, M. Ishimatsu, T. Yanuki, N. Arima, and M. Arii, "Creep Crack Propagation in Aluminum-Copper-Magnesium Alloy," Proc. of Symp. on Mechanical Behavior of Materials, Kyoto, 1974, 467-477.

8. R. Koterazawa, "On the Applicability of Linear Elastic Fracture Mechanics to Creep Crack Propagation," Int. Journal of Fracture, 11 (1975), 1060-1062.

9. J. D. Landes and R. P. Wei, "Kinetics of Subcritical Crack Growth in a High Strength Steel," Trans. ASME, J. Basic Eng. Mater. Tech., 95 (1973), 2-9.

10. T. Kawaskai and M. Horiguchi, "Creep Crack Propagation in Austenitic Steels at Elevated Temperatures," Eng. Fracture Mech., 9 (1977), 879-889.

11. J. R. Haigh, "The Mechanisms of Macroscopic High Temperature Crack Growth Part II: Review and Re-Analysis of Previous Work," Mater. Sci. and Eng., 20 (1975), 225-235.

REFERENCES (CONTINUED)

12. P. E. Irving and L. N. McCartney, "Prediction of Fatigue Crack Growth Rates: Theory, Mechanisms and Experimental Results," Met. Sci., 11 (1977), 351-361.

13. R. D. Nicholson and C. L. Formby, "The Validity of Various Fracture Mechanics Methods at Creep Temperatures," Int. Journal of Fracture, 11 (1975), 595-604.

14. R. D. Nicholson, "The Effect of Temperature on Creep Crack Propagation in AISI 316 Stainless Steel," Mater. Sci. and Eng., 22 (1976), 1-6.

15. J. R. Haigh, "The Mechanisms of Macroscopic High Temperature Crack Growth Part I: Experiments on Tempered Cr-Mo-V Steels," Mater. Sci. and Eng., 20 (1975), 213-223.

16. A. A. Wells and F. H. McBride, "Application of Fracture Mechanics to High Temperature Creep Rupture," Canadian Metallurgical Quarterly, 6 (1967), 347-368.

17. R. Pilkington, D. Hutchinson, and C. L. Jones, "High-Temperature Crack-Opening Displacement Measurements in a Ferritic Steel," Metal Science, 8 (1974), 237-241.

18. S. Floreen and R. H. Kane, "A Critical Strain Model for the Creep Fracture of Nickel-Base Superalloys," Met. Trans., 7A (1976), 1157-1160.

19. J. M. Larson and S. Floreen, Metallurgical Factors Affecting Crack Growth Resistance of a Superalloy," Met. Trans., 8A (1977), 51-55.

20. J. T. Barnby, "Crack Tip Stresses Under Steady State Creep," Eng. Fracture Mech., 6 (1974), 627-630.

21. J. T. Barnby, "Crack Propagation During Steady State Creep," Eng. Fracture Mech., 7 (1975), 299-304.

22. V. Vitek, "A Theory of the Initiation of Creep Crack Growth," Int. Journal of Fracture, 13 (1977), 39-50.

REFERENCES (CONTINUED)

23. V. Vitek, "A Fracture Mechanics Theory of Creep Crack Growth," Central Electricity Research Laboratories Report No. RD/L/R 1953, 1977.

24. D. J. Gooch, J. R. Haigh, and B. L. King, "Relationship Between Engineering and Metallurgical Factors in Creep Crack Growth," Metal Science, 11 (1977), 545-550.

25. J. M. Larsen, "An Investigation of the Shape and Extent of Crack Tip Plastic Zones in Fatigue Crack Propagation and the Role of the Overload Plastic Zone in Retardation," M.S. Thesis, Vanderbilt University, Nashville, Tenn., 1977.

26. J. Lankford, D. L. Davidson, and T. S. Cook, "Fatigue Crack Tip Plasticity," ASTM STP 637, Philadelphia, 1977, pp. 36-55.

27. P. F. Packman, "Role of Interferometry in Fracture Studies," in Experimental Techniques in Fracture Mechanics, A. S. Kobayashi, ed., Iowa State University Press, Ames 1975, pp. 59-83.

28. J. S. Ke and H. W. Liu, "Thickness Effect on Crack Tip Deformation at Fracture, Dept. of Chemical Engineering and Materials Science, Syracuse University, Syracuse, New York, August 1974.

29. J. H. Underwood and D. P. Kendall, "Measurement of Microscopic Plastic-Strain Distributions in the Region of a Crack Tip," Exp. Mech., July (1969), 296-304.

30. J. S. Ke and H. W. Liu, "Near Tip Strain as a Ductile Fracture Criterion," Int. J. of Fracture Mech., 7 (1971), 487-490.

31. W. Elber, Engineering Fracture Mechanics, 2 (1970), 37-45.

32. J. W. Jones, D. E. Macha, and D. M. Corbly, "Observations on Fatigue Crack Opening Load Determinations," Int. J. of Fracture, 14 (1978), R25-R30.

33. D. E. Macha, D. M. Corbly, and J. W. Jones, "On the Variation of Fatigue Crack Opening Load with Measurement Location," accepted for publication in Experimental Mechanics.

REFERENCES (CONTINUED)

34. J. R. Rice, J. Appl. Mech., 34 (197), 287.

35. S. Ikeda, Y. Izumi, and M. E. Fine, "Plastic Work During Fatigue Crack Propagation in a High Strength Low Alloy Steel and in 7050 Al Alloy," Eng. Fracture Mech., 9 (1977), 123-136

36. A. J. Durelli and V. J. Parks, Moiré Analysis of Strain, Prentice-Hall, Inc., Englewood Cliffs, N.J., 1970.

37. R. D. Dudderar and R. O'Regan, "Measurement of the Strain Field Near a Crack Tip in Polymethylmethacrylate by Holographic Interferometry," Exp. Mech., Feb. 1971, p. 49-56.

☆U.S.Government Printing Office: 1979 — 657-002/613